Title

The Ufd1 cofactor determines the linkage specificity of polyubiquitin chain engagement by the AAA+ ATPase Cdc48

Journal

Molecular Cell, 83(5)

ISSN

1097-2765

Authors

Williams, Cameron

Dong, Ken C

Arkinson, Connor

et al.

Publication Date

2023-03-01

DOI

10.1016/j.molcel.2023.01.016

Peer reviewed

Published in final edited form as:

Mol Cell. 2023 March 02; 83(5): 759–769.e7. doi:10.1016/j.molcel.2023.01.016.

The Ufd1 cofactor determines the linkage specificity of polyubiquitin chain engagement by the AAA+ ATPase Cdc48

Cameron Williams[1,2], **Ken C Dong**[2,3,4], **Connor Arkinson**[2,3,4], **Andreas Martin**[2,3,4,5,*]

[1]Biophysics Graduate Group, University of California, Berkeley, CA 94720, USA.

[2]California Institute for Quantitative Biosciences, University of California at Berkeley, Berkeley, CA 94720, USA

[3]Department of Molecular and Cell Biology, University of California at Berkeley, Berkeley, CA 94720, USA

[4]Howard Hughes Medical Institute, University of California at Berkeley, Berkeley CA, 94720

[5]Lead contact

Summary

The AAA+ ATPase Cdc48 utilizes the cofactor Ufd1/Npl4 to bind and thread polyubiquitinated substrates for their extraction from complexes or membranes and often for subsequent proteasomal degradation. Previous studies indicated that Cdc48 engages polyubiquitin chains through the Npl4-mediated unfolding of an initiator ubiquitin, yet the underlying principles remain largely unknown. Using FRET-based assays, we revealed the mechanisms and kinetics of ubiquitin unfolding, insertion into the ATPase, and unfolding of the ubiquitin-attached substrate. We found that Cdc48 uses Ufd1's UT3 domain to bind a K48-linked ubiquitin on the initiator's proximal side of the chain, thereby directing the initiator toward rapid unfolding by Npl4 and engagement by Cdc48. Ubiquitins on the initiator's distal side increase substrate affinity and facilitate unfolding, but impede substrate release from Cdc48-Ufd1/Npl4 in the absence of additional cofactors. Our findings explain how Cdc48-UN efficiently processes substrates with K48-linked chains of 4-6 ubiquitins, which represent most cellular polyubiquitinated proteins.

Graphical Abstract

*Correspondence should be addressed to A.M. (a.martin@berkeley.edu).

Author Contributions:

Conceptualization, C.W. and A.M.; Methodology, C.W. and A.M.; Investigation, C.W., K.C.D., and C.A.; Writing – Original Draft, C.W. and A.M.; Writing – Review & Editing, C.W., A.M., K.C.D., and C.A.; Funding Acquisition, A.M.; Supervision, A.M.

Declaration of Interests:

The authors declare no competing interests.

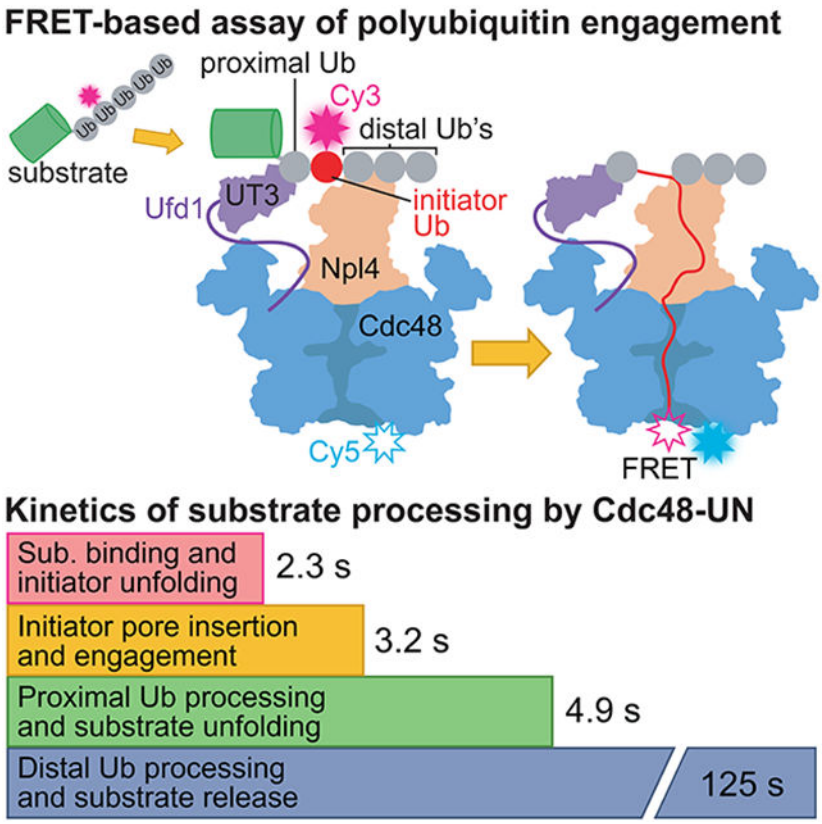

eTOC Blurb:

The AAA+ ATPase Cdc48/p97 mobilizes polyubiquitinated proteins from macromolecular assemblies or membranes for their proteasomal degradation. Using fluorescence-based assays, Williams et al. show how Cdc48's Ufd1/Npl4 cofactor is utilized for engaging substrate-attached polyubiquitin chains in a length-, linkage-, and position-specific manner for mechanical substrate processing by the ATPase motor.

Introduction

The AAA+ ATPase Cdc48 in yeast (or p97/VCP in metazoans) performs diverse functions in all eukaryotic cells by extracting polyubiquitinated clients from membranes, protein assemblies, and chromatin, often delivering them to the 26S proteasome for degradation [1]. The most well-studied pathway involving Cdc48/p97 is the endoplasmic reticulum-associated degradation (ERAD), where Cdc48/p97 removes misfolded proteins from the ER membrane for proteasomal turnover [2]. Consistent with the central role of Cdc48/p97 in protein homeostasis, mutations in human p97 are directly linked to neurodegenerative diseases [3] and its upregulation is observed in some cancers [4]. Cdc48/p97 is composed of an N-terminal domain (N domain) and two contiguous AAA+ ATPase domains, D1 and D2, that hexamerize to form a double ring with a central channel. Many cofactor proteins assist Cdc48/p97 in recognizing and unfolding its substrates [5], and one of the most prevalent is the heterodimeric cofactor Ufd1/Npl4 (UN), which binds to the D1 (or cis) face of the hexamer

and recruits substrates by interacting with their attached polyubiquitin chains. Previous proteomics studies revealed a strong preference of Cdc48/p97-UN for K48-linked chains [6], with more than 90 % of cellular substrates bearing this linkage type [7]. Once delivered to Cdc48/p97, a substrate is engaged by the ATPase motor, and ATP-hydrolysis-driven motions of the AAA+ domains mechanically translocate the polypeptide through the central channel, causing it to unfold [7-9].

Unlike the related AAA+ motor of the 26S proteasome that engages ubiquitinated substrates through an unstructured tail or internal flexible loop of the substrate protein itself [10-13], Cdc48 in complex with the UN cofactor (Cdc48-UN) initiates substrate processing through engagement of the attached polyubiquitin chain [7]. Cryo-EM structures of ATP-hydrolysis-incompetent Cdc48-UN and a polyubiquitinated substrate revealed key features of this ubiquitin engagement and the initiation of translocation [14], whereby an unfolded “initiator” ubiquitin is bound to the groove-like surface of the Npl4 cofactor subunit, with its N-terminus inserted into the Cdc48 central channel. Also visible in these structures were two folded K48-linked ubiquitin moieties attached to the K48 residue of the initiator and thus on the distal side of the chain, interacting with the top of Npl4. However, neither any ubiquitins besides the three Npl4-bound moieties nor the UT3 domain of Ufd1, which has previously been shown to interact with ubiquitin chains [15], were resolved. These data led to a model in which a polyubiquitinated substrate is recruited to Cdc48 through ubiquitin binding to the two sites on top of Npl4 and possibly additional sites on Ufd1, before an initiator ubiquitin moiety somewhere in the chain unfolds, is captured by the Npl4 groove, and inserts its N terminus into the Cdc48 central channel for engagement by conserved pore loops of the D1 and D2 ATPase domains (Fig. 1A). Ensuing biochemical studies indicated that ATP hydrolysis-driven motions of the ATPase domains subsequently translocate the initiator ubiquitin, any additional ubiquitin moieties on its proximal side, and the attached substrate protein, leading to their mechanical unfolding, while ubiquitins distal to the initiator may be spared from unfolding and get released or passed through a lateral seam in the Cdc48 hexameric ring [7].

However, the key principles underlying substrate engagement and translocation by Cdc48-UN are still unclear. While previous studies reported rates for model-substrate unfolding [16], the kinetics of initial ubiquitin unfolding and engagement remain unknown, and the rate-limiting step of substrate processing has yet to be identified. One of the most fascinating aspects of polyubiquitin-chain engagement by Cdc48-UN is the selection of the initiator with regards to its position in a polyubiquitin chain as well as the determinants for the apparent K48-linkage preference. Previous cryo-EM structures were solved using substrates with long, non-uniform chains, which made it impossible to identify which ubiquitin served as an initiator and how many ubiquitins were flanking it on either side. Only three ubiquitins were visible bound to Npl4 in the initiation state of Cdc48-UN [14], yet previous biochemical studies had to employ substrates with very long or branched chains to see robust unfolding [9,16], such that the length requirements for ubiquitin-chain processing are unknown. Furthermore, based on experiments with truncation mutants of Ufd1 it was proposed that ubiquitin binding to the UT3 domain is critical for substrate recruitment to Cdc48-UN [7], but the underlying principles and what roles Ufd1 may play in engagement, unfolding, and the linkage-specific selection of ubiquitin chains remained unclear.

Here, we use fluorescence- and FRET-based assays to reveal a complete kinetic picture and key mechanistic details of ubiquitin-chain engagement and translocation by Cdc48-UN, characterize the chain-length dependence and rate-limiting step of substrate processing, and identify Ufd1's UT3 domain as a proximal ubiquitin sensor that determines the linkage specificity of Cdc48-UN.

Results

Cdc48-UN rapidly engages polyubiquitin chains in an ATP-hydrolysis independent manner

To monitor the individual steps of polyubiquitin-chain engagement by Cdc48, we sought to develop separate FRET-based assays for initiator-ubiquitin unfolding and insertion into the channel. A previous study on the conformations of ubiquitins within a K48-linked dimer used a donor-acceptor FRET pair [17], and we aimed to employ a similar assay to detect the Cdc48-UN-mediated unfolding of an initiator ubiquitin in the context of a K48-linked chain. Polyubiquitin chains for these FRET-based studies were constructed by extending a N-terminally Cy3-labeled ubiquitin with a chain of K48-linked ubiquitins whose N-termini were conjugated to Cy5 (^{Cy3}Ub-^{Cy5}Ub$_n$, with (−) representing a K48-linked isopeptide bond between a proximal and a distal ubiquitin; Fig. 1B). Since the distance between the N-termini of K48-linked ubiquitins is ~ 45 Å [18] and thus comparable to the Förster radius for a Cy3-Cy5 FRET pair, high FRET efficiency is expected between the Cy3 donor dye on the first, most proximal ubiquitin and the Cy5 acceptor dye on the second ubiquitin moiety in the chain. To confirm this, we cleaved ^{Cy3}Ub-^{Cy5}Ub$_n$ with the deubiquitinase USP2 into monomeric Cy3- and Cy5-labeled ubiquitins and observed an increase in Cy3 fluorescence as well as a reciprocal decrease in Cy5 fluorescence, consistent with the presence of a high-FRET efficiency state in the assembled chains (Fig. S1A). The magnitude of the Cy5-fluorescence decrease was rather modest due to the presence of only a single Cy3 donor and an excess of Cy5 acceptor-labeled ubiquitins, which, furthermore, get to some extent directly excited during excitation of the donor at 480 nm.

If either the first or second ubiquitin in the chain served as an initiator and unfolded upon binding to Npl4, the distance between the Cy3 and Cy5 dyes would significantly increase and lead to a low-FRET efficiency state. Indeed, incubation of ^{Cy3}Ub-^{Cy5}Ub$_n$ with an excess of Cdc48-UN complex, but not with the motor or UN cofactor alone, in the presence of the non-hydrolyzable ATP analog ATPγS caused a decrease in steady-state FRET efficiency, as evidenced by an increase in Cy3 fluorescence (Fig. 1C). As a control, polyubiquitin chains lacking Cy5 acceptor labels on distal ubiquitins (^{Cy3}Ub-Ub$_n$) did not display an appreciable increase in Cy3 donor fluorescence upon incubation with Cdc48-UN (Fig. S1B), which is consistent with the Cy3 fluorescence being a reliable indicator of FRET for the ^{Cy3}Ub-^{Cy5}Ub$_n$ construct. To further verify that the decrease in FRET efficiency originated from unfolding of an initiator ubiquitin and not a conformational change of the entire chain upon interaction with the binding sites on top of Npl4, we incubated ^{Cy3}Ub-^{Cy5}Ub$_n$ with Cdc48-UN complexes containing the previously reported W252A/R253E or D460K/Y461A double mutations in the ubiquitin-binding groove of Npl4 [14]. Consistent with this groove's role in interacting with the unfolded initiator ubiquitin, both double-mutant Cdc48-UN complexes

failed to produce significant increases in donor-fluorescence levels of ^{Cy3}Ub-^{Cy5}Ub$_n$ chains (Fig. 1D, S1C).

Next, we measured the timing of the combined steps of ubiquitin-chain binding and initiator unfolding by mixing ^{Cy3}Ub-^{Cy5}Ub$_n$ with an excess of Cdc48-UN bound to ATPγS in a stopped-flow instrument and monitoring the increase in Cy3 fluorescence over time. We observed a double exponential increase in donor fluorescence, with a time constant of $\tau_{bind+unfold}$ = 2.7 ± 0.2 s for the fast phase (Fig. 1E and Table 1). The slow phase, which accounts for ~ 50 % of the total signal change, likely originates from a population of motor-cofactor complexes that are in a conformation less suitable for rapid initiator unfolding. Similar curves and initiator-unfolding rates were observed for ATP-hydrolysis deficient Cdc48 variants with Walker-B mutations in their D1 or D2 domains (E315Q and E588Q, respectively). Interestingly, ^{Cy3}Ub-^{Cy5}Ub$_n$ chains incubated with wild-type Cdc48-UN in the presence of ATP displayed a single-exponential increase in Cy3 fluorescence with a time constant of $\tau_{bind+unfold}$ = 2.3 ± 0.2 s. The faster kinetics and the lack of a slow phase for this sample suggest that actively ATP-hydrolyzing Cdc48 motors better support initiator unfolding, potentially due to differences in their N-domain conformations, which depend on the nucleotide state of Cdc48 subunits [19,20] and affect cofactor binding and orientation [21]. Another explanation for the effect of ATP hydrolysis on the observed kinetics for initiator unfolding is that the change in FRET efficiency may reach a maximum amplitude once the N-terminus of ubiquitin is fully inserted into Cdc48's central channel, and ATPase-driven translocation accelerates this process. Indeed, a translocation-compromised double mutant in which both aromatic residues in the grip-conferring pore loops of the D2 ATPase domain were mutated to alanines (W561A/Y562A) also displayed slower kinetics with two phases (Fig. 1E). To directly observe the insertion of the initiator ubiquitin into the Cdc48 motor, we developed another FRET-based assay that reads out the proximity between a Cy3-donor dye on the N-terminus of the initiator ubiquitin and a Cy5-acceptor dye at the bottom of the Cdc48 processing channel. We constructed chains in which only the second ubiquitin was N-terminally labeled with Cy3 (Ub-^{Cy3}Ub-Ub$_n$) and incorporated the unnatural amino acid 4-azido-L-phenylalanine (AzF) at position D602 in the D2 pore-2 loop of Cdc48 for labeling with Cy5-DBCO [22]. Based on the structural information for ubiquitin-engaged Cdc48-UN [14], the initiator's N-terminus in the central channel is less than 26 Å away from D602 in any of the six Cdc48 protomers, such that insertion of a Cy3-labeled ubiquitin moiety into the Cy5-labeled motor should lead to a significant increase in FRET efficiency (Fig. S1D). Addition of UN to a mixture of Ub-^{Cy3}Ub-Ub$_n$ and excess ^{Cy5}Cdc48 in ATPγS showed a robust decrease in Cy3-donor fluorescence and an increase in Cy5-acceptor fluorescence (Fig. 1F). Similar to the FRET-based initiator-unfolding assay described above, the magnitude of increases in Cy5-acceptor fluorescence for the pore-insertion assay were rather modest due to the overabundance of acceptor dyes relative to donor dyes when using excess concentrations of Cdc48 with multiple Cy5 labels per hexamer. Importantly, the Cy3 fluorescence intensity of Ub-^{Cy3}Ub-Ub$_n$ remained unchanged when UN was added in the absence of ^{Cy5}Cdc48 and even slightly increased upon addition of unlabeled ^{AzF}Cdc48-UN, indicating that the observed Cy3-fluorescence quenching in the presence of ^{Cy5}Cdc48-UN indeed originates from bona fide FRET (Fig. S1E). Furthermore, robust Cy3 quenching

depended on an intact, non-mutated Npl4 groove (Fig. 1G, S1F), which further supports that the assay reports on the insertion of the initiator ubiquitin into Cdc48.

To gain insight into the relative timing of individual steps during polyubiquitin engagement, we sought to measure pore-insertion kinetics for comparison with the kinetics observed in the initiator-unfolding assay. Stopped-flow mixing experiments for the pore-insertion assay in ATPγS, which reports on the combined kinetics for polyubiquitin-chain binding, initiator unfolding, and insertion into Cdc48, showed a double exponential decrease of Cy3 fluorescence, with a time constant for the fast phase of $\tau_{bind+unfold+insert}$ = 3.2 ± 0.1 s (Fig. 1H). This time constant is similar to the one measured in the initiator-unfolding assay ($\tau_{bind+unfold}$ = 2.7 ± 0.2 s, Fig. 1E), suggesting that ubiquitin unfolding is rate-limiting for engagement by Cdc48.

A proximal ubiquitin is necessary for initiator engagement

After observing pore insertion of an initiator ubiquitin at the second position in a K48-linked chain, we wondered whether the most proximal ubiquitin could also serve as an initiator. Surprisingly, when chains with a Cy3 label on the first ubiquitin (^{Cy3}Ub-Ub$_n$, Fig. S2A) were mixed with ^{Cy5}Cdc48-UN, no Cy3 fluorescence change was detected (Fig. 2, S2B), prompting us to explore the basis for positional selectivity of initiator ubiquitins. We first tested whether the most proximal ubiquitin in a chain could function as an initiator if it is attached to another polypeptide, similar to the scenario found in a polyubiquitinated protein substrate. However, when analyzing K48-linked chains in which the most proximal ubiquitin was C-terminally fused to an SH3 domain from mouse c-Crk, we observed Cy3-fluorescence quenching only when the dye was attached to the N-terminus of the second, but not the first ubiquitin moiety (Fig. 2, S2B). Recognition by Cdc48-UN apparently requires the initiator ubiquitin to be linked to another ubiquitin on its proximal side. To investigate the importance of the linkage type for this recognition, we fused the N-terminus of a SH3-domain attached ubiquitin to the C-terminus of a Cy3-labeled, second ubiquitin, which in turn was extended by a K48-linked chain. This construct allowed us to assess whether a ubiquitin distal to a linear M1-linkage could serve as an initiator. Interestingly, no Cy3 fluorescence quenching was observed when these M1/K48 mixed linkage chains were incubated with ^{Cy5}Cdc48-UN, unless the Cy3 dye was moved from the second to the third moiety, and thus to the distal side of the first K48 linkage in the chain (Fig. 2, S2B). Taken together, our results indicate that robust engagement requires the initiator ubiquitin to be preceded by a proximal ubiquitin, which is likely preferred to have a K48-linkage.

The UT3 domain of Ufd1 is the proximal ubiquitin sensor

We hypothesized that Cdc48-UN may interact with the ubiquitin proximal to the initiator through the UT3 domain of Ufd1 (Fig. 3A), which was previously shown in isolation to bind mono- and polyubiquitin [15]. Since there is no structural model available for ubiquitin-bound UT3, we generated an AlphaFold model for the UT3-ubiquitin complex (Fig. 3A, S3). Based on this model, the canonical I44 patch of ubiquitin interacts with Ufd1's well-conserved L55 (Fig. S4A), which is located in an area of the UT3-domain surface that displayed chemical shift perturbations in a previous NMR study of ubiquitin binding [15]. To disrupt this potential ubiquitin-binding interface, we generated a Ufd1 L55R mutant. Ufd1^{L55R} showed normal

complex formation with Npl4 (Fig. S4B) and Cdc48, leading to a suppression of Cdc48's ATPase activity to a similar extent and with similar affinity (K_D = 0.5 μM) as wild-type UN (K_D = 1.0 μM Fig. S4C). Importantly, Cdc48-Ufd1^{L55R}/Npl4 exhibited significant defects in initiator-ubiquitin unfolding and pore insertion when tested in our FRET-based assays with ^{Cy3}Ub-^{Cy5}Ub$_n$ or with Ub-^{Cy3}Ub-Ub$_n$ and ^{Cy5}Cdc48, respectively (Fig. S4D, 3B, S4E), indicating that UT3 binding of the K48-linked ubiquitin proximal to the initiator is important for unfolding initiation by Cdc48-UN. We could rule out that the UT3 domain interacts with distal ubiquitins or the initiator ubiquitin itself, because Ub^{I44A}-^{Cy3}Ub-Ub$_n$, containing an I44A mutation in the most proximal ubiquitin, also showed a defect for pore insertion of the Cy3-labeled initiator ubiquitin in the second position (Fig. 3C, S4F). For a more direct readout of this interaction between the UT3 domain and the ubiquitin moiety proximal to the initiator, we designed another FRET-based assay, using a Cy3-donor dye attached to a N-terminal cysteine in the most proximal ubiquitin of Ub$_4$ (^{Cy3}Ub-Ub$_3$) and a Cy5-acceptor dye attached to a cysteine replacing R64 in UT3. Based on our AlphaFold model for the UT3-ubiquitin complex, position 64 in UT3 is solvent-exposed and ~20 Å away from the N-terminus of a bound ubiquitin (Fig. 3A). In addition to the engineered C64, Ufd1 contains two native cysteines (C27 and C186), but neither one is solvent-exposed, and wild-type Ufd1 accordingly did not get labeled in control experiments. When we mixed ^{Cy3}Ub-Ub$_3$ and ^{Cy5}Ufd1/Npl4 with an excess of Cdc48 in ATPγS, we observed a decrease in Cy3 fluorescence and a reciprocal increase in Cy5 fluorescence (Fig. 3D), indicating a direct interaction between the proximal ubiquitin and UT3. No appreciable increases in FRET efficiency were detected in the presence of the ubiquitin-binding incompetent ^{Cy5}Ufd1^{L55R} mutant (Fig. 3E), and additional controls showed no significant change in the Cy3 fluorescence of ^{Cy3}Ub-Ub$_n$ when mixed with unlabeled Cdc48-UN (Fig. S1B) and also no change in the Cy5 fluorescence of ^{Cy5}UN upon addition of Cdc48 in the absence of ^{Cy3}Ub-Ub$_3$ (Fig. S4G). In summary, we can conclude that Ufd1's UT3 domain interacts with the ubiquitin moiety proximal to the initiator ubiquitin and functions as a sensor for the chain linkage in this position, rather than binding moieties on the distal side as previously proposed [7,14].

Distal ubiquitins bind Npl4 to ensure robust initiator insertion

Given our findings about the requirement for a ubiquitin moiety on the proximal side of the initiator, we wondered whether a K48-linked dimer represents the lower bound regarding the chain length necessary for engagement by Cdc48-UN and what roles ubiquitins distal to the initiator might play. To purify ubiquitin chains of various lengths for pore-insertion experiments, we fractionated the heterogeneous Ub-^{Cy3}Ub-Ub$_n$ chains by size exclusion chromatography (SEC) (Fig. S5A). While the mostly Ub-^{Cy3}Ub-containing fraction showed only minor Cy3 quenching when mixed with excess ^{Cy5}Cdc48-UN in the presence of ATPγS (Fig. 4A), fractions with higher proportions of Ub-^{Cy3}Ub-Ub$_2$ tetrameric or longer chains displayed 5-7-fold larger signal changes (Fig. 4A), suggesting that ubiquitins distal to the initiator increase a chain's affinity for Npl4 and/or facilitate initiator unfolding and Cdc48 insertion. This is consistent with previous structural studies that revealed two ubiquitin moieties bound to sites at the top of the Npl4 cofactor, in addition to the unfolded initiator interacting with the Npl4 groove [14].

To assess whether the same chain-length trends hold true for the processing of a polyubiquitinated substrate and how substrate-unfolding kinetics compare to initiator-engagement kinetics, we built a library of substrates with defined ubiquitin-chain lengths ranging from Ub_1 to Ub_6 and the most-proximal ubiquitin C-terminally fused to the N-terminus of the green fluorescent protein mEos3.2 (Eos~Ub_n, with (~) representing a linear fusion between the N-terminus of Eos and the C-terminus of the most proximal ubiquitin in a chain; Fig. S5B,C). Eos reversibly loses fluorescence upon unfolding and translocation by Cdc48 [9,16]. Under single-turnover conditions with 10 μM Cdc48-UN in the presence of an ATP regeneration system, appreciable substrate unfolding was observed for substrates of all chain lengths except Ub_1, which lacks a second ubiquitin moiety to fulfill the initiation requirements of binding Ufd1's UT3 domain and Npl4's unfolding groove (Fig. 4B). Time constants for the fast phase were determined by double-exponential fitting of the Eos-fluorescence traces and inversely correlated with ubiquitin-chain lengths, reaching a minimum of $\tau_{\text{Eos unfold}} = 4.4 \pm 0.1$ s for Ub_6-Eos (Table 2), which is more than an order of magnitude faster than any previously reported substrate unfolding by Cdc48 or p97. This time constant for the combined binding, initiation, and unfolding of the Eos~Ub_6 substrate, together with the time constant measured for initiator-ubiquitin binding and unfolding by Cdc48-UN in ATP ($\tau_{\text{bind+unfold}} = 2.3 \pm 0.2$ s) and the assumption of a sequential reaction scheme, let us estimate a time constant for processing of the proximal ubiquitin-chain and unraveling of the Eos moiety ($\tau_{\text{Ub process.}} \sim 2.0$ s), as well as a lower bound for Cdc48's translocation velocity. Upon unfolding and pore insertion of the second ubiquitin as the first possible initiator moiety in the chain, Cdc48 needs to translocate ~ 92 residues to reach Eos for unfolding (58 residues of the initiator that are outside of the Cdc48 pore at the time of N-terminal insertion; 29 residues for the proximal ubiquitin, from its initiator-linked Lys48 to the C-terminal Gly76 that is fused to the Eos linker; and 5 residues for the linker between ubiquitin and Eos, Fig. S1D, S5B). Cdc48 thus appears to translocate its substrate with a velocity of at least 45 residues per second, which is an underestimate considering that the onset of translocation and the mechanical unfolding of the proximal ubiquitin moiety likely require additional time.

Interestingly, the single-turnover unfolding measurements of Eos substrates with defined ubiquitin chains showed a sharp acceleration when the chain length increased from Ub_3 to Ub_4, which further supports the hypothesis that occupying both ubiquitin binding sites on top of Npl4 enhances engagement of the initiator ubiquitin and substrate processing. Indeed, we found that disrupting these two ubiquitin-binding sites with the Npl4 T255A/T571A double mutation leads to considerably slower Eos~Ub_4 unfolding that resembles the unfolding kinetics of Eos~Ub_2 (Fig. 4C). The minimal substrate Eos~Ub_2 is expected to engage with Cdc48-UN in only a single register, with the first ubiquitin contacting Ufd1's UT3 domain and the second ubiquitin functioning as the initiator. Consistently, no single-turnover unfolding of Eos~Ub_2 was detected for Cdc48-Ufd1^{L55R}/Npl4 with a ubiquitin-binding incompetent UT3 domain (Fig. 4D), and Eos~Ub_2 unfolding was independent of the ubiquitin-binding sites on top of Npl4 when using Cdc48-Ufd1/Npl4$^{T255A/T571A}$ (Fig. S5D). To further assess the contributions of the Npl4 ubiquitin-binding sites to substrate affinity and unfolding initiation, we performed Michaelis-Menten analyses of multiple-turnover Eos unfolding. For these steady-state measurements, we transformed the green fluorescent

Eos~Ub_2, Eos~Ub_4, and Eos~Ub_5 substrates into their red fluorescent counterparts by UV irradiation, which cleaves the backbone of mEos3.2 and makes unfolding irreversible [16,23]. In initial control experiments to verify similar behavior of Eos^{red} and Eos^{green}, we simultaneously monitored the single-turnover unfolding of the green and red fractions of photoconverted Eos~Ub_4 and observed nearly identical fast-phase velocities (τ_{red} = 7.6 ± 2.8 s, τ_{green} = 7.9 ± 0.8 s; Fig. S6A), which confirmed Eos^{red} as a well-suited substrate for our Michaelis-Menten analyses. Multiple-turnover unfolding of Eos^{red}~Ub_2 and Eos^{red}~Ub_4 revealed K_M values of 4.1 ± 0.7 μM and 0.41 ± 0.08 μM, respectively (Fig. S6B), indicating that the absence of distal ubiquitins in Eos^{red}~Ub_2 to interact with the binding sites on top of Npl4 lowers the substrate affinity by a factor of 10. The v_{max} for Eos^{red}~Ub_2 unfolding was found to be 0.63 ± 0.03 min^{-1}, which is equivalent to a time constant of τ = 95 ± 5 s (Fig. S6B; Table 2) and in good agreement with the time constant for the single-turnover unfolding of this substrate (τ_{fast} = 79.3 ± 2.3, Table 2). Based on this ~ 18-fold slower unfolding compared the single-turnover unfolding of Eos^{red}~Ub_6 (τ_{fast} = 4.4 ± 0.1, Table 2), we can conclude that initiation is rate-limiting for Eos^{red}~Ub_2 processing and that interactions of distal ubiquitins with the binding sites on top of Npl4 play an important role for efficient initiator insertion into the central channel.

However, in contrast to Eos~Ub_2 that showed a nice agreement of single- and multiple-turnover unfolding kinetics, the rates for the multiple-turnover processing of Eos^{red}~Ub_4 and Eos^{red}~Ub_5 were about an order of magnitude lower than the rates for their single turnover (Table 2). Michaelis-Menten analyses for Eos^{red}~Ub_4 unfolding showed tight substrate binding (K_M = 0.41 ± 0.08 μM), but slow multiple-turnover processing with v_{max} = 0.64 ± 0.03 min^{-1} or τ = 94 ± 4 s, ~ 7-fold slower than under single-turnover conditions (Fig. S6B; Table 2). A process other than initiator insertion or Eos unfolding must therefore be rate-limiting for the multiple turnover of substrates with chains of four or more ubiquitins. To rule out that unraveling of a non-fluorescent unfolding intermediate or translocation of the unfolded Eos polypeptide represent the slow step, we fused a mTurquoise2 moiety to the C-terminus of mEos3.2 in a Turquoise~Eos~Ub_4 substrate (with (~) representing a N-to-C-terminal fusion of Turquoise, Eos, and ubiquitin moieties), allowing us to read out the completion of Eos processing through the loss of Turquoise fluorescence. Fitting the Turquoise fluorescence change upon Turquoise~Eos~Ub_4 unfolding by Cdc48-UN under single-turnover conditions with a lagged exponential function gave a time constant of $\tau_{Eos\ process.}$ = 25.6 ± 2.2 s for the lag and $\tau_{Turq.\ unfold}$ = 9.8 ± 0.8 s (Fig. S7A). The lag includes initiator insertion, unfolding of the proximal ubiquitin, Eos unfolding, and complete Eos translocation, and is considerably faster than the multiple-turnover processing of Eos~Ub_4. Substrate release from Cdc48 is therefore the likely reason for slow turnover, as previous work by others also suggested that Cdc48 cannot rapidly unfold and translocate distal ubiquitins [7]. Instead, a substrate may exit laterally from the central channel or require deubiquitination by Otu1 to liberate inhibitory distal ubiquitins on the cis side of the motor. For processing toward the proximal side of an initiator ubiquitin moiety located at position 2 of a chain, the K48 branchpoint of this initiator has to enter the Cdc48 channel far enough to make contact with the pore loops in the D2 ATPase domain, which requires the immediately distal 3rd ubiquitin to be unfolded as well. To assess whether Cdc48-UN is able to unfold any subsequent ubiquitins on the distal side, we used a substrate

with mEos3.2 fused to the N-terminus of the distal ubiquitin in a K48-linked tetrameric chain (Ub_4~Eos). Consistent with previous findings, multiple-turnover measurements of this substrate after photoconversion showed no significant decrease in red Eos fluorescence (Fig. S7B), indicating that ubiquitin moieties two positions distal from the initiator are not rapidly unfolded by Cdc48-UN.

This lack of distal ubiquitin unfolding and translocation is expected to slow down substrate release and thus represent the rate-limiting step for multiple-turnover unfolding by Cdc48-UN and for substrate degradation in the case of Cdc48-coupled proteolysis by the 26S proteasome. To test this, we switched back to the canonical geometry with Eos attached to the proximal end of the ubiquitin chain in Eos~Ub_5 and incubated this substrate with Cdc48-UN to reach a steady state of Eos unfolding and refolding before adding the 26S proteasome for degradation (Fig. 4E). At the point of proteasome addition, there should be a pool of Cdc48-processed substrate that at least equates the concentration of Cdc48-UN in the reaction (2 μM) and thus is at saturating levels for proteasomal binding and turnover. The actual degradation rate, however, depends on whether this pool of Eos~Ub_5 is still bound to Cdc48-UN or released and available for immediate proteasome binding. We observed a time constant for proteasomal degradation of 162 ± 18 s, which is similar to the time constant of 125 ± 4 s for the multiple-turnover unfolding of Eos^{red}~Ub_5 by Cdc48-UN (Table 2). This result is thus consistent with release from Cdc48-UN indeed being the rate-limiting step of processing for substrates with more than three ubiquitins.

Discussion

Cdc48-UN is a versatile protein unfoldase that acts on a broad range of ubiquitinated substrates. It was recently revealed that the site of engagement is the polyubiquitin signal itself [14], which explains how Cdc48 can process a structurally highly diverse set of substrates. However, the determinants for engagement and processing were still not well understood. Here, we reveal critical mechanistic principles of polyubiquitin binding, engagement, and translocation by Cdc48-UN, as well as its apparent preference for K48-linked chains and the kinetics of individual steps. A previous study used hydrogen-deuterium exchange with mass spectrometry to detect polyubiquitin unfolding by Cdc48-UN complexes in an endpoint assay [7], which did not track individual ubiquitins in a chain. Employing time-resolved FRET-based assays, we found that an initiator ubiquitin rapidly unfolds by binding to the UN cofactor and inserts within ~ 3 seconds into the pore of the Cdc48 hexamer in a manner independent of ATP-hydrolysis. Moreover, using site-specific fluorescence labeling we were able to probe how ubiquitin moieties at different positions in a polyubiquitin chain insert into Cdc48, revealing that an initiator ubiquitin must be preceded by a proximal ubiquitin in a K48-linked chain.

Both Npl4 and Ufd1 contain multiple ubiquitin binding sites [15,24], but their individual contributions to substrate engagement remained unclear. In this study, we delineated the distinct roles of Ufd1 and Npl4 for the initiation of ubiquitin unfolding. The UT3 domain of Ufd1 plays the essential role of sensing an ubiquitin with a likely preference for K48 linkage and facilitating the Npl4-mediated insertion of the immediately distal moiety into the Cdc48 pore. Processing of our minimal substrate modified with a ubiquitin dimer demonstrates

that this binding register, involving Ufd1's UT3 domain and Npl4's unfolding groove, is dominant over ubiquitin interactions with the additional sites on top of Npl4 and thus appear to dictate the apparent K48-linkage specificity of Cdc48-UN.

Previous *in vitro* studies required substrates with long ubiquitin chains to observe robust Cdc48/p97-UN unfoldase activity [7-9]. While a ubiquitin dimer was sufficient for substrate processing in our study, we detected rapid unfolding with tetrameric chains and maximal rates for substrates with chains of five or six ubiquitins, in nice agreement with the lengths typically observed for polyubiquitinated proteins *in vivo* [25]. For these chains with 4-6 ubiquitins, we found that interactions of the two ubiquitins on the distal side of the initiator with the sites on top of Npl4 not only increase a substrate's affinity for Cdc48-UN, but also appear to help positioning the initiator ubiquitin for pore insertion. Our data lead to a Cdc48-engagement model (Fig. 5) where Ufd1 and Npl4 each grasp one or two ubiquitins flanking an initiator moiety that thereby gets positioned for rapid unfolding and insertion into the motor pore. Cdc48 then quickly translocates the initiator ubiquitin, which is coupled to unfolding of a single ubiquitin immediately distal to the initiator. The motor subsequently unfolds and translocates any proximally located ubiquitin moieties with a velocity of at least 45 residues per second to reach the attached substrate protein for unfolding. Substrate release from Cdc48-UN, rather than the start of translocation as previously suggested [7], represents the slow step of processing. This slow substrate release is likely caused by distal ubiquitins, which appear to not get threaded through Cdc48, but remain on the cis side of the motor. The partially translocated ubiquitin chain therefore must either laterally exit the Cdc48 channel through a seam in the hexamer or slide backwards out of the pore and pull the substrate protein with it. A more likely release mechanism *in vivo* is the trimming of distal ubiquitins on the motor's cis side by the deubiquitinase Otu1, which has been previously shown to release stalled substrates with long ubiquitin chains from Cdc48 [9]. Considering that Cdc48-UN can engage and unfold an ubiquitinated substrate like mEos3.2 in less than 5 s, eliminating the rate-limiting substrate-release step through Otu1-mediated cleavage of distal ubiquitins might allow *in vivo* processing of substrates to occur in just a few seconds and thus much faster than previously assumed.

Cdc48-UN is able to rapidly process ubiquitin moieties on the proximal side of the initiator and unfold an attached substrate protein within a few seconds, likely because it pulls on these ubiquitins through their Lys48 side chains, whereas ubiquitins on the distal side are pulled on through their C-terminus (Fig. S7C). Previous single-molecule atomic force microscopy studies showed that the mechanical stability of ubiquitin is much lower when a pulling force is applied through Lys48 versus the C-terminus [26]. The UT3-mediated apparent specificity for K48-linked ubiquitins proximal to the initiator may therefore provide an additional advantage for rapid mechanical unfolding by Cdc48-UN.

Our finding that ubiquitin interactions with sites on both Ufd1 and Npl4 are essential for robust substrate processing raises the question whether there are additional ubiquitin-binding sites on UN or Cdc48 itself that may play a role in engagement. Previous NMR studies showed that different surfaces on the UT3 domain of isolated Ufd1 are involved in binding monoubiquitin versus polyubiquitin chains [15], suggesting that Ufd1 could interact with more than one ubiquitin on the proximal side of the initiator. Interestingly, the N-domain of

Cdc48/p97 contains the same double Ψ barrel fold as the UT3 domain [15], and human p97 was shown to bind polyubiquitin chains directly [27]. Cdc48's N-domains may thus interact with ubiquitins proximal or distal to the initiator and thereby aid in substrate processing.

Besides UN as one of the most important adaptors of Cdc48/p97, there exist many other ubiquitin-binding cofactors [5], yet whether those could mediate polyubiquitin-chain engagement through a mechanism similar to Cdc48-UN remains unknown. Cofactor-bound Cdc48/p97 has also been shown to act on an increasing number of substrates modified with proteins of the ubiquitin-like (Ubl) family, such as SUMO, NEDD8, and Atg8, and it is unclear whether engagement in these cases occurs through the Ubl domains themselves. Our FRET-based engagement assays provide powerful tools not only for studying polyubiquitin engagement by Cdc48-UN in greater detail, but also for exploring how Cdc48/p97 collaborates with other cofactors to recognize and remodel polyubiquitinated or Ubl-modified substrates.

Limitations of the study

Previous proteomics and biochemical studies established a strong preference of Cdc48/p97-UN for substrates with K48-linked chains [6,7] and an inability to efficiently recognize M1 or K63 linkages [9]. Based on our findings, binding of Ufd1's UT3 domain to the ubiquitin moiety located proximal to the initiator is likely responsible for this K48-linkage preference. However, we did not explicitly test K6, K11, K27, K29, or K33 linkages to rule out that they could mediate some level of Cdc48-UN unfolding despite their low abundance on cellular substrates.

Also, further experiments are required to elucidate the mechanisms of substrate release from Cdc48/p97 and the processing, remodeling, or Out1/YOD1-mediated cleavage of distal moieties in a substrate-attached ubiquitin chain. In addition, the underlying principles for substrate transfer from Cdc48/p97 to the 26S proteasome, potentially facilitated by shuttle factors, remain largely elusive.

STAR Methods

RESOURCE AVAILABILITY

Lead contact—Further information and requests for resources and reagents should be directed to and will be fulfilled by the lead contact, Andreas Martin (a.martin@berkeley.edu).

Materials availability—All constructs generated in this study are available from the lead contact upon request and completion of a Material Transfer Agreement.

Data and Code Availability:

- All data generated or analyzed during this study are included in this manuscript and the Supplementary Data. Original SDS PAGE images scanned for Cy3/C5 fluorescence or Coomassie stain are deposited at Mendeley and are publicly

available. The DOI (doi:10.17632/65dyy7tkny.1) is also listed in the resources table.

- This paper does not report original code.
- Any additional information required to reanalyze the data reported in this paper is available from the lead contact upon request.

EXPERIMENTAL MODEL AND SUBJECT DETAILS

E. coli BL21 star (DE3) cells were transformed with vectors for the respective constructs, grown in phosphate-buffered Terrific Broth at 37 °C until OD_{600} = 1.0, and induced with 1 mM IPTG overnight at 18 °C.

METHOD DETAILS

Purification of Cdc48 and ^{AzF}Cdc48—Cdc48, D1 and D2 Walker B mutants (E315Q and E588Q, respectively), and the D2 pore loop double mutant (W561A/Y562A) were expressed and purified as previously described [16]. Briefly, cells were harvested by centrifugation at 3,500 rcf and resuspended in NiA buffer (60 mM HEPES, pH 7.6, 200 mM NaCl, 20 mM imidazole, and 10 mM $MgCl_2$) supplemented with 1 mM ATP, DNase I, lysozyme, and protease inhibitors. Following sonication, the lysate was clarified by centrifugation at 27,000 rcf and added to Ni-NTA beads (Thermo Scientific). Beads were washed with NiA plus 1 mM ATP, and Cdc48 was eluted with NiA plus 1 mM ATP and 350 mM imidazole. PreScission protease was added to the resulting eluate, which was then incubated overnight at 4 °C to remove the N-terminal His_6-tag on Cdc48. The high imidazole buffer was exchanged for NiA plus 1 mM ATP the following day by repeated concentrated and dilution. A subtractive IMAC step was performed to remove uncleaved Cdc48 and His_6-PreScission. Further purification of the flow-through was achieved by size exclusion chromatography using a Superose 6 XK 16/70 column equilibrated in GF buffer plus ATP. Due to the presence of 1 mM ATP, which absorbs at 280 nm, protein concentration was determined by a Bradford assay (Biorad).

Cdc48 bearing AzF at position Glu602 was expressed using a similar protocol to the one previously reported for the recombinant expression of yeast 26S proteasome subcomplexes [28]. Briefly, 3 L of BL21 star (DE3) expression cells were grown in phosphate-buffered Terrific Broth at 37 °C to an OD of 0.4. Cells were harvested by centrifugation at 3,500 rcf and resuspended in 1 L of media containing 2 mM AzidoPhenylalanine (AzF, Acrotein ChemBio Inc.). The resulting 1 L culture was induced overnight at 18 °C with 1 mM isopropyl β-D-thiogalactopyranoside (IPTG) and harvested the following day by centrifugation. Cell pellets were resuspended in NiA buffer with added DNase I, lysozyme, and protease inhibitors (aprotinin, pepstatin, leupeptin, and PMSF). Cells were sonicated, and the resulting lysate was clarified by centrifugation at 27,000 rcf. The rest of the purification was identical to that of wild-type Cdc48.

Purification of Ufd1/Npl4 and individual cofactor proteins—Ufd1/Npl4 heterodimers containing wild-type Npl4 or Npl4 initiator binding groove double mutants (W252A/R253E and D460K/Y461A) were expressed and purified as previously described

[16]. Briefly, cells were harvested by centrifugation at 3,500 rcf and resuspended in NiA buffer with added DNase I, lysozyme, and protease inhibitors. After sonication, the lysate was clarified by centrifugation at 27,000 rcf and incubated with Ni-NTA. Beads were washed with NiA, and proteins were eluted with NiA plus 350 mM imidazole. Eluate was treated with PreScission protease overnight at 4 °C to remove the C-terminal His_6-tag on Ufd1, and the high imidazole buffer was exchanged for NiA the next day by repeated concentrated and dilution. A subtractive IMAC step was performed to remove uncleaved UN and His_6-PreScission. The flow-through was further purified by size exclusion chromatography using a Superdex 200 16/600 column equilibrated in GF buffer.

Wild-type Ufd1, Ufd1 bearing a UT3 ubiquitin binding mutation (L55R), and Ufd1 bearing a cysteine mutation for labeling (R64C) were expressed and purified in the absence of Npl4. Growths and subsequent purification steps were done in the exact same way as they were performed for the co-expressed and co-purified Ufd1/Npl4 constructs. Wild-type Npl4 and the Npl4 ubiquitin binding tower double mutant (T255A/T571A) were also purified in the absence of Ufd1. The growths and purifications were done in a similar manner to those for the co-purified Ufd1/Npl4 constructs, except the purifications were performed using a N-terminal His_6-GST tag on Npl4 or Npl4 T255A/T571A.

Purification of ubiquitin and MC-ubiquitin—Untagged wild-type ubiquitin and ubiquitin with a cysteine inserted before the first methionine of the native sequence (MC-ubiquitin) were expressed and purified as previously described, except acetic acid was used in place of perchloric acid for the precipitation steps (Worden et al., 2014). Briefly, cells were harvested by centrifugation at 3,500 rcf, and the resulting pellets were resuspended in NiA with added with added DNase I, lysozyme, and protease inhibitors. Sonication was used to lyse cells, and further clarification was achieved by centrifugation at 27,000 rcf. Contaminating proteins other than ubiquitin in the supernatant were precipitated by addition of glacial acetic acid until a pH of 4.5 was reached. The solution was stirred for 30 min and clarified by centrifugation at 27,000 rcf. To remove salt, the supernatant was dialyzed twice against 4 L cation buffer A (50 mM NaOAc pH 4.5) for 2 h each. The solution was again clarified by centrifugation at 27,000rcf to remove precipitated proteins. The resulting supernatant was filtered and loaded onto a 5 mL HiTrap SP FF cation exchange chromatography column (Cytiva) equilibrated with cation buffer A. Ubiquitin constructs were eluted from the column by a 0 mM to 350 mM NaCl gradient over 20 column volumes. Fractions containing ubiquitin were concentrated and subjected to size exclusion chromatography using a Superdex 75 16/600 column equilibrated in GF buffer for further purification.

Cells expressing C-terminally MC-Ub, MC-Ub^{I44A}, MC-Ub-SH3, and MC-Ub-Ub^{K48R}-SH3 in addition N-terminally His-tagged Ub^{K48R} were harvested by centrifugation at 3,500 rcf and resuspended in NiA buffer with added DNase I, lysozyme, and protease inhibitors. Following sonication, lysate was clarified by centrifugation at 27,000 rcf, and the resulting supernatant was incubated with Ni-NTA. Beads were washed with NiA, and proteins were eluted with NiA plus 350 mM imidazole. The eluate was concentrated with a 3 kDa spin filter and subjected to size exclusion chromatography using a Superdex 75 16/600 column equilibrated in GF buffer.

Purification of ubiquitin-Eos and ubiquitin-Eos-Turquoise fusions—The linear fusion of ubiquitin and mEos3.2 (with ubiquitin C-terminally fused to the N-terminus of the green fluorescent protein mEos3.2, denoted as Eos~Ub) and the linear fusion of ubiquitin, mEos3.2, and mTurquoise2 (Turquoise~Eos~Ub) were expressed and purified in the same way as previously described for the tetraubiquitin fusion, Eos~Ub_4 [16]. Briefly, cells were harvested by centrifugation at 3,500 rcf, and the resulting pellets were resuspended in NiA buffer with added DNase I and protease inhibitors. Cells were lysed by sonication, and the resulting lysate was clarified by centrifugation at 27,000 rcf and mixed with Ni-NTA. Following washes with NiA, protein was eluted from the column with NiA plus 350 mM imidazole. The N-terminal His_6-SUMO tag on ubiquitin was cleaved by treatment with SENP2 protease overnight at 4 °C. Following repeated concentration and dilution to exchange the high imidazole buffer for NiA, a subtractive IMAC step removed His_6-SUMO, His_6-SENP2, and uncleaved Eos~Ub or Turquoise~Eos~Ub. The flow-through was incubated with chitin resin (NEB), and the C-terminal intein-CBD tag was cleaved on column with GF plus 50 mM DTT. The eluate was then subjected to further purification by size exclusion chromatography using a Superdex 75 16/600 column equilibrated in GF buffer.

Purification of the E2-E3 chimera gp78RING-Ube2g2—The E2-E3 chimera gp78RING-Ube2g2 was expressed and purified as previously described [8]. Briefly, cells were harvested by centrifugation, resuspended in NiA with added DNase I, lysozyme, and protease inhibitors, and lysed by sonication, and the lysate was clarified by centrifugation at 27,000 rcf. The supernatant was added to Ni-NTA, and the beads were washed with NiA. The protein was eluted with NiA plus 350 mM imidazole, and the eluate was treated with TEV protease overnight at 4 °C to cleave the N-terminal His_6-tag. The high imidazole buffer was exchanged for NiA by repeated concentration and dilution, and a subtractive IMAC step was used to remove uncleaved gp78RING-Ube2g2 and His-tagged TEV. Further purification was achieved by size exclusion chromatography using a Superdex 75 16/600 column equilibrated in GF buffer.

Purification of Ube1, SENP2, Cdc34, USP2, PreScission protease, and TEV protease—Mouse E1 (Ube1), SENP2, Cdc34, USP2, PreScission protease, and TEV protease were expressed and purified as previously described [10,29-31]. pET28-mE1 was a gift from Jorge Eduardo Azevedo (Addgene plasmid # 32534), pET28a-SENP2 (catalytic domain) was a gift from Guy Salvesen (Addgene plasmid # 16357), and USP2 was a gift from Cheryl Arrowsmith (Addgene plasmid # 36894). Cultures were harvested by centrifugation, resuspended in NiA with added DNase I, lysozyme, and protease inhibitors, lysed by sonication, and clarified by centrifugation at 27,000 rcf. The supernatants were added to Ni-NTA, and the beads were washed with NiA. Proteins were eluted with NiA plus 350 mM imidazole and further purified by size exclusion chromatography using a Superdex 75 16/600 (SENP2, USP2, Cdc34) or a Superdex 200 16/600 (Ube1) equilibrated in GF buffer.

Conjugating Cy3/Cy5 to ubiquitin and Cy5 to Ufd1—MC-ubiquitin and its derivatives were labeled with Cy3 or Cy5 dyes at the N-terminal cysteine. First, 50 μM of

MC-ubiquitin constructs were incubated with 1 mM TCEP to reduce cysteines and improve labeling efficiency. Next, a 10-fold excess of sulfo-Cy3-maleimide or sulfo-Cy5-maleimide (Lumiprobe) was added and labeling was carried out for 30 min at room temperature in buffer (25 mM HEPES pH 7.4, 150 mM NaCl). The reaction was quenched with 5 mM DTT and subjected to size-exclusion chromatography with a Superdex 75 increase 10/300 column equilibrated in GF buffer. Protein concentration was quantified based on Cy3 or Cy5 absorbance. Ufd1 was conjugated to Cy5 under similar conditions as ubiquitin, except the cysteine for maleimide labeling was incorporated in place of Arg64 located in the UT3 domain. Our labeling is site-specific, because the two native cysteines of Ufd1 (Cys27 and Cys186), which appear buried in an NMR structure, were not amenable to labeling when we reacted Cy5 with wild-type Ufd1 lacking the R64C mutation. Protein concentration was quantified based on Cy5 absorbance.

Conjugating Cy5 to Cdc48—Cdc48 was conjugated to Cy5 through the unnatural amino acid AzF incorporated at Asp604 using a procedure to the one previously reported for labeling of the base and lid subcomplexes of the 26S proteasome [28]. First, 10 μM (hexamer) of $Cdc48^{D602AzF}$ was incubated with 1 mM 5,5'-dithiobis-(2-nitrobenzoic acid) (DTNB) in GF buffer plus 1 mM ATP at room temperature for 10 min to reversibly block solvent exposed cysteines from off-target modification. Next, dibenzocyclooctyne (DBCO) conjugated Cy5 (Lumiprobe) was added to a concentration 200 μM, and the reaction was incubated at room temperature for 2-3 hr. Excess Cy5-DBCO was then quenched by the addition of 2 mM AzF. Finally, DTNB-modified cysteines were returned to free cysteines using 5 mM DTT, and the mixture was subjected to size exclusion chromatography using a Superose 6 increase 10/300 column equilibrated in GF buffer plus 1 mM ATP. Labeling efficiencies were determined by measuring the concentration of Cy5 by absorbance and Cdc48 concentration by Bradford assay.

Assembly of ubiquitin chains for FRET studies—K48-linked ^{Cy3}Ub-^{Cy5}Ub$_n$ polyubiquitin chains (written proximal-to-distal) were assembled by incubating a mixture of ^{Cy3}Ub-His$_6$ and ^{Cy5}Ub with ubiquitination machinery (His$_6$-E1 and the E2-E3 fusion, gp78RING-Ube2g2) at 37 °C for 30 min in buffer (20 mM HEPES pH 7.4, 10 mM $MgCl_2$, 0.5 mM DTT, and 10 mM ATP). Final concentrations were 35 μM ^{Cy3}Ub-His$_6$, 350 μM ^{Cy5}Ub, 1 μM His$_6$-E1, and 20 μM gp78RING-Ube2g2. The reaction was diluted with NiA buffer and passed over Ni-NTA resin to selectively capture His-tagged ^{Cy3}Ub-^{Cy5}Ub$_n$, while untagged gp78RING-Ube2g2 and any off-target ^{Cy5}Ub$_n$ remained in the flow-through. The Cy3/Cy5-labeled chains were eluted with NiB buffer and concentrated using a spin filter (MWCO 3 kDa). Protein concentration was quantified based on Cy3 absorbance. ^{Cy3}Ub-Ub$_n$ chains were assembled in the same way as described above, except that the mixture contained unlabeled ubiquitin in place of ^{Cy5}Ub. SH3~^{Cy3}Ub-Ub$_n$ and SH3~Ub~^{Cy3}Ub-Ub$_n$ chains were assembled from $SH3^{His6}$~^{Cy3}Ub and $SH3^{His6}$~Ub^{K48R}~^{Cy3}Ub, respectively.

To prepare Ub-^{Cy3}Ub-Ub$_n$, SH3~Ub-^{Cy3}Ub-Ub$_n$, and SH3~Ub~Ub-^{Cy3}Ub-Ub$_n$ chains, the first step was to generate Ub-^{Cy3}Ub, SH3~Ub-^{Cy3}Ub, and SH3~Ub~Ub-^{Cy3}Ub. Ub-His$_6$, $SH3^{His6}$~Ub, or $SH3^{His6}$~Ub^{K48R}~Ub were mixed with a limiting amount of ^{Cy3}Ub in the presence of ubiquitination machinery and incubated at 37 °C for 30 min in buffer (20 mM

HEPES pH 7.4, 10 mM $MgCl_2$, 0.5 mM DTT, and 10 mM ATP). Final concentrations were 50 μM Ub-His_6 (or SH3 derivatives), 5 μM ^{Cy3}Ub, 1 μM His_6-E1, and 20 μM gp78RING-Ube2g2. The reaction was diluted with NiA buffer and passed over Ni-NTA resin to selectively capture His-tagged chains, while untagged gp78RING-Ube2g2 and any off-target $^{Cy3}Ub_n$ chains remained in the flow-through. The Cy3-labeled dimers were eluted with NiB buffer, concentrated using a spin filter (MWCO 3 kDa), and further purified by size-exclusion chromatography with a Superdex 75 increase 10/300 column equilibrated in GF buffer. Longer chains of dye-free ubiquitin were then assembled on Ub-^{Cy3}Ub, SH3~Ub-^{Cy3}Ub, and SH3~Ub~Ub-^{Cy3}Ub. Final concentrations were 25 μM Ub-^{Cy3}Ub (or SH3 derivatives), 125 μM^{Cy3}Ub, 1 μM His_6-E1, and 20 μM gp78RING-Ube2g2. The reaction was diluted with NiA buffer and passed over Ni-NTA resin to selectively capture His-tagged Ub-^{Cy3}Ub-Ub_n (or SH3 derivatives), while tag-less gp78RING-Ube2g2 and any off-target Ub_n chains that formed remained in the flow-through. The Cy3-labeled chains were eluted with NiB buffer and concentrated using a spin filter (MWCO 3 kDa). Protein concentration was quantified based on Cy3 absorbance.

FRET-based initiator-unfolding and pore-insertion assays—Steady-state FRET assays of initiator unfolding and pore insertion were performed in a BMG Labtech CLARIOstar plate reader at 30 °C. Polyubiquitin chains (Cy3/Cy5-labeled for initiator unfolding or Cy3-labeled for pore insertion) were mixed with excess Cdc48 (unlabeled for initiator unfolding or Cy5-labeled for pore insertion) and UN in assay buffer (60 mM HEPES, pH 7.6, 75 mM NaCl, 75 mM KCl, 10 mM $MgCl_2$, 0.5 mg/mL BSA) with 1 mM ATPγS. Final concentrations for initiator unfolding assays were 0.2 μM Cy3/Cy5-chains, 2 μM Cdc48, and 10 μM UN. Final concentrations for pore insertion assays were 0.2 μM Cy3/Cy5-chains, 2 μM Cdc48, and 2 μM UN. The mixtures were transferred in a total volume of 10 μL into a preheated 384-well black plate (Costar) and incubated for 2 minutes at 30 °C. An excitation wavelength of 480 nm was used, and spectra were generated by performing a fluorescence emission scan from 525 nm to 725 nm. The degree to which the donor emission was quenched was used to measure pore insertion. In the case of ubiquitin unfolding, an increase in donor emission was monitored. The following equation was used to calculate percent changes in donor fluorescence for both the initiator unfolding and pore insertion assays:

$$\%\ change\ in\ donor\ emission = \frac{\left| I_{D,\ -UN} - I_{D,\ +UN} \right|}{I_{D,\ -UN}} \times 100$$

The kinetics of initiator unfolding and pore insertion were measured in an Auto SF120 stopped-flow fluorimeter (Kintek). The stopped-flow was loaded with 145 μL of 2X polyubiquitin chains (Cy3/Cy5-labeled for initiator unfolding or Cy3-labeled for pore insertion) and 145 μL of 2X Cdc48 (unlabeled for initiator unfolding or Cy5-labeled for pore insertion) and UN. Final concentrations for initiator unfolding kinetics were 0.2 μM Cy3/Cy5-chains, 5 μM Cdc48, and 5 μM UN. Final concentrations for pore insertion assays were 0.2 μM Cy3/Cy5-chains, 2 μM Cdc48, and 2 μM UN. The buffer conditions, which included 1 mM ATPγS, were the same as those used in the plate reader. After loading the samples, four blank shots were fired, followed by three measurements. An excitation wavelength of

480 nm was used, and Cy3 and Cy5 emission channels were measured simultaneously. The decrease or increase in the Cy3 fluorescence signal was fit to a double exponential.

FRET-based UT3-binding assay—The steady-state FRET-based assay for monitoring ubiquitin binding to Ufd1 UT3 was performed in a similar way as the initiator-unfolding and pore-insertion assays, but differed in the labeled components and their final concentrations. K48-linked Ub_4 chains with Cy3 conjugated to the first, most proximal ubiquitin were mixed in assay buffer containing 1 mM ATPγS with excess Cdc48 and UN, in which Ufd1's UT3 domain was labeled on Cys64 with Cy5. Final concentrations were 0.2 μM ^{Cy3}Ub-Ub_3, 2 μM Cdc48, and 2 μM ^{Cy5}UN. Steady-state levels of FRET efficiency were calculated using the following equation:

$$FRET\ efficiency = \frac{I_{\text{acceptor}}}{I_{\text{donor}} + I_{\text{acceptor}}}$$

The percent change in FRET efficiency was calculated using the following equation:

$$\%\ change\ in\ FRET = \frac{FRET_{+\text{Cdc48}} - FRET_{-\text{Cdc48}}}{FRET_{-\text{Cdc48}}} \times 100$$

Preparation of Eos and Turquoise~Eos substrates with defined ubiquitin lengths—To prepare Eos substrates with defined ubiquitin chain lengths, we first purified K48-linked Ub_2, Ub_3, and Ub_4 chains as previously described [32]. Each chain, along with mono Ub, was then extended with a single Ub^{K48R} moiety using gp78RING-Ube2g2 to form Ub-Ub^{K48R}, Ub_2-Ub^{K48R}, Ub_3-Ub^{K48R}, and Ub_4-Ub^{K48R}. The reactions were carried out for 30 min at 37 °C with 50 μM Ub_n, 100 μM His_6-Ub^{K48R}, 1 μM His_6-E1, and 20 μM gp78RING-Ube2g2 in buffer (20 mM HEPES pH 7.4, 10 mM $MgCl_2$, 0.5 mM DTT, and 10 mM ATP). Following dilution with NiA buffer, the reactions were passed over Ni-NTA resin. His-tagged Ub_n-Ub^{K48R} and excess unreacted Ub^{K48R} were bound to the resin, while tag-less gp78RING-Ube2g2 remained in the flow-through. The NiB eluate was subjected to size-exclusion chromatography with a Superdex 75 increase 10/300 column equilibrated in GF buffer to purify Ub_n-Ub^{K48R} from Ub^{K48R}.

To form Eos~Ub_2, Eos~Ub_3, Eos~Ub_4, Eos~Ub_5, and Eos~Ub_6, Ub_n-Ub^{K48R} or Ub^{K48R} were mixed with Eos~Ub in the presence of ubiquitination machinery and reacted at 37 °C for 30 min in buffer (20 mM HEPES pH 7.4, 10 mM $MgCl_2$, 0.5 mM DTT, and 10 mM ATP). The concentrations were 50 μM Eos~Ub, 40 μM His-tagged Ub_n-Ub^{K48R} or Ub^{K48R}, 1 μM His_6-E1, and 20 μM gp78RING-Ube2g2. Reactions were diluted with NiA buffer and passed over Ni-NTA to capture His-tagged Eos~Ub_n, while tag-less gp78RING-Ube2g2 remained in the flow-through. Substrates were eluted from Ni-NTA with NiB buffer and concentrated and diluted into GF buffer. Concentrations were quantified based on Eos absorbance. Turqoise~Eos~Ub_4 was purified in the same way as Eos~Ub_4, except Ub_2-Ub^{K48R} was mixed with Turquoise~Eos~Ub in the presence of the ubiquitination machinery.

The Ub_4~Eos substrate, with Eos fused to the N-terminus of the most distal ubiquitin, was prepared by reacting His_6-Eos-Ub^{K48R} (where (−) represents the linear fusion between

Eos' C-terminus and ubiquitin's N-terminus) with Ub_3 under the same conditions as above, except that His_6-Eos-Ub^{K48R} and Ub_3 were both at 50 μM.

Photoconversion of Eos substrates—Eos~Ub, Eos~Ub_4, and Eos~Ub_5 were photoactivated for 1 h on ice using Blak-Ray model B-100AP UV lamp with a 100 watt 365 nm bulb to convert a fraction of substrates from green to red fluorescence. Following irradiation, the concentration of red fluorescent species was ~ 30 – 40 % of the total concentration of fluorescent species (green Eos plus red Eos).

Single-turnover Eos and Turquoise~Eos unfolding assays—Single-turnover Eos-unfolding assays were performed in a QuantaMaster spectrofluorometer (PTI) at 30 °C. Ubiquitin-modified Eos substrates were preincubated with ATP regeneration mix and creatine phosphate in assay buffer. Cdc48 and UN were preincubated with ATP regeneration mix, creatine phosphate, and BSA in assay buffer. Unfolding was initiated by mixing Eos~Ub_n and Cdc48-UN samples in a preheated 1.5 cm quartz cuvette (Hellma). The final concentrations were 0.5 μM Eos~Ub_n substrate, 10 μM Cdc48-UN, 0.5 mg/mL BSA, 100 mM creatine phosphate, and 1X ATP regeneration mix (5 mM ATP, 0.03 mg/ml creatine kinase and 16 mM creatine phosphate). Unfolding of green Eos was monitored by the loss of fluorescence at 520 nm after excitation at 500 nm, and photoconverted red Eos was monitored at 585 nm after excitation at 565 nm. Single-turnover unfolding of Turquoise~Eos~Ub_4 was performed in the same way as described above, except Turquoise unfolding was monitored by the loss of fluorescence at 475 nm after excitation at 415 nm.

Assuming a sequential reaction scheme consisting of initiator binding and engagement (with a rate constant $k_{bind+unfold}$) followed by processing of the proximal part of the ubiquitin chain and unraveling of the Eos moiety (with a rate constant $k_{Ub\ process}$), the observed decay of the Eos fluorescence signal during Ub_n-Eos substrate processing under single-turnover conditions is described by:

$$Eos(t) = Eos(0)\left(1 - \left(\frac{\left(k_{\text{Ub process}} - k_{\text{Ub process}} \cdot e^{-k_{\text{bind+unfold}} \cdot t}\right) - \left(k_{\text{bind+unfold}} - k_{\text{bind+unfold}} \cdot e^{-k_{\text{Ub process}} \cdot t}\right)}{k_{\text{bind+unfold}} - k_{\text{Ub process}}}\right)\right)$$

For our system and the experimental conditions, this Eos fluorescence decay can be well approximated and fit by a single- or double-exponential decay function, and in case of the photoconverted red Eos by a double-exponential decay plus linear funtion. In our analyses of Eos~Ub_n processing we only considered the dominant fast phase (with $k_{Eos\ unfold}$), whereas the slow phase showed varying lower or no amplitudes and may originate from a sub-population of conformationally distinct substrates. The rate for proximal ubiquitin-chain processing and Eos unraveling ($k_{Ub\ process}$) can thus be determined as:

$$k_{\text{Ub process}} = \frac{k_{\text{Eos}\,unfold} \cdot k_{\text{bind+unfold}}}{k_{\text{Eos}\,unfold} - k_{\text{bind+unfold}}}$$

Unfolding of the Turquoise moiety in the Turquoise~Eos~Ub_4 substrate by Cdc48-UN can be described by a lagged double-exponential

$$Turqoise(t) = A_1 \cdot e^{-k_1 \cdot t \cdot (1 - e^{-k_0 \cdot t})} + A_2 \cdot e^{-k_2 \cdot t \cdot (1 - e^{-k_0 \cdot t})} + c$$

In this equation, k_1 and k_2 represent the fast and slow rate constants of the Turquoise fluorescence decay, and k_0 represents the delay in Turquoise unfolding, originating from the combined steps of initiator binding and engagement, proximal ubiquitin processing, Eos unfolding, and Eos translocation.

Multiple-turnover Eos unfolding assays—Multiple-turnover assays of photoconverted Eos~Ub_n were performed using a BMG Labtech CLARIOstar plate reader at 30 °C. Photoconverted Eos~Ub, Eos~Ub_4, and Eos~Ub_5 were mixed with Cdc48, UN, BSA, and ATP regeneration mix in assay buffer. The final concentrations were 0.1 μM Cdc48, 5 μM UN, 0.5 mg/mL BSA, and 1X ATP regeneration mix. Eos~Ub_2 unfolding was measured at increasing concentrations of up to 40 μM, Eos~Ub_4 was titrated up to 10 μM, Eos~Ub_5 unfolding was measured at a single concentration of 2.5 μM. For all these substrates, unfolding was monitored by measuring the loss of red Eos fluorescence at 585 nm after excitation at 565 nm. Rates of unfolding were determined by fitting the linear steady-state portions of the traces. Michaelis-Menten analysis was performed by the fitting the initial velocities of red Eos fluorescence decay (v_0) at varying Eos~Ub_n concentrations to the equation:

$$\frac{v_0}{[Cdc48]} = \frac{k_{cat} \cdot [Eos \sim Ub_n]}{K_M + [Eos \sim Ub_n]}$$

Multiple-turnover unfolding of photoconverted Ub_4~Eos^{red} with Eos fused to the N-terminus of the distal ubiquitin was measured in a similar manner as described above, but with Ub_4~Eos and UN at 2.5 μM.

ATPase assays—ATP hydrolysis rates were determined using a spectrophotometric assay that couples the formation of ADP to the depletion of NADH upon ATP regeneration (Nørby, 1988). Measurements were performed in a BMG Labtech CLARIOstar plate reader. Cdc48 (with and without Npl4 or Ufd1 and the Ufd1-L55R mutant) and ATPase mix were preincubated separately at 30 °C and then combined in a preheated 384-well clear bottom plate. Absorbance at 340 nm was monitored over time. Cdc48 was present at a final concentration of 0.05 μM and Ufd1/Npl4, $Ufd1^{L55R}$/Npl4, or Npl4 alone were present at final concentrations up to 10 μM for titration reactions to determine the co-factor affinity for Cdc48. Reactions were performed in 1X ATPase mix (5 mM ATP, 3 U mL^{-1} pyruvate kinase (Sigma), 3 U mL^{-1} lactate dehydrogenase (Sigma), 1 mM NADH, 7.5 mM phosphoenol pyruvate (Sigma)) and assay buffer. ATPase rates were determined from the linear region of the absorbance trace.

Co-elution of Ufd1 and Npl4 by size exclusion chromatography—Samples containing different compositions of Ufd1, $Ufd1^{L55R}$, and Npl4 were prepared and

subjected to size-exclusion chromatography using a Superdex 200 increase 10/300 column equilibrated in GF buffer. Final concentrations were 40 μM Ufd1 and 40 μM Npl4.

QUANTIFICATION AND STATISTICAL ANALYSIS

Details about the statistical analyses for individual experiments, including the statistical tests and exact values of N (number of technical replicates), can be found in the figure legends. Error bars represent the mean ± S.D.

Supplementary Material

Refer to Web version on PubMed Central for supplementary material.

Acknowledgements:

We thank the members of the Martin lab for helpful discussions.

Funding:

This research was funded by the Howard Hughes Medical Institute (K.C.D., C.A., A.M.) and by the US National Institutes of Health (R01-GM094497 to A.M.).

References

1. van den Boom J, and Meyer H (2018). VCP/p97-Mediated Unfolding as a Principle in Protein Homeostasis and Signaling. Mol Cell 69, 182–194. 10.1016/j.molcel.2017.10.028. [PubMed: 29153394]
2. Wolf DH, and Stolz A (2012). The Cdc48 machine in endoplasmic reticulum associated protein degradation. Biochim Biophys Acta 1823, 117–124. 10.1016/j.bbamcr.2011.09.002. [PubMed: 21945179]
3. Meyer H, and Weihl CC (2014). The VCP/p97 system at a glance: connecting cellular function to disease pathogenesis. J Cell Sci 127, 3877–3883. 10.1242/jcs.093831. [PubMed: 25146396]
4. Deshaies RJ (2014). Proteotoxic crisis, the ubiquitin-proteasome system, and cancer therapy. BMC Biol 12, 94. 10.1186/s12915-014-0094-0. [PubMed: 25385277]
5. Hanzelmann P, and Schindelin H (2017). The Interplay of Cofactor Interactions and Post-translational Modifications in the Regulation of the AAA+ ATPase p97. Front Mol Biosci 4, 21. 10.3389/fmolb.2017.00021. [PubMed: 28451587]
6. Tsuchiya H, Ohtake F, Arai N, Kaiho A, Yasuda S, Tanaka K, and Saeki Y (2017). In Vivo Ubiquitin Linkage-type Analysis Reveals that the Cdc48-Rad23/Dsk2 Axis Contributes to K48-Linked Chain Specificity of the Proteasome. Molecular Cell 66, 488–502.e487. 10.1016/j.molcel.2017.04.024. [PubMed: 28525741]
7. Ji Z, Li H, Peterle D, Paulo JA, Ficarro SB, Wales TE, Marto JA, Gygi SP, Engen JR, and Rapoport TA (2022). Translocation of polyubiquitinated protein substrates by the hexameric Cdc48 ATPase. Mol Cell 82, 570–584 e578. 10.1016/j.molcel.2021.11.033. [PubMed: 34951965]
8. Blythe EE, Olson KC, Chau V, and Deshaies RJ (2017). Ubiquitin- and ATP-dependent unfoldase activity of P97/VCP*NPLOC4*UFD1L is enhanced by a mutation that causes multisystem proteinopathy. Proc Natl Acad Sci U S A 114, E4380–E4388. 10.1073/pnas.1706205114. [PubMed: 28512218]
9. Bodnar NO, and Rapoport TA (2017). Molecular Mechanism of Substrate Processing by the Cdc48 ATPase Complex. Cell 169, 722–735 e729. 10.1016/j.cell.2017.04.020. [PubMed: 28475898]
10. Bard JAM, Bashore C, Dong KC, and Martin A (2019). The 26S Proteasome Utilizes a Kinetic Gateway to Prioritize Substrate Degradation. Cell 177, 286–298 e215. 10.1016/j.cell.2019.02.031. [PubMed: 30929903]

11. Fishbain S, Prakash S, Herrig A, Elsasser S, and Matouschek A (2011). Rad23 escapes degradation because it lacks a proteasome initiation region. Nature communications 2, 192. 10.1038/ncomms1194.
12. Inobe T, Fishbain S, Prakash S, and Matouschek A (2011). Defining the geometry of the two-component proteasome degron. Nature Chemical Biology 7, 161–167. 10.1038/nchembio.521. [PubMed: 21278740]
13. Schrader EK, Harstad KG, and Matouschek A (2009). Targeting proteins for degradation. Nat Chem Biol 5, 815–822. 10.1038/nchembio.250. [PubMed: 19841631]
14. Twomey EC, Ji Z, Wales TE, Bodnar NO, Ficarro SB, Marto JA, Engen JR, and Rapoport TA (2019). Substrate processing by the Cdc48 ATPase complex is initiated by ubiquitin unfolding. Science 365. 10.1126/science.aax1033.
15. Park S, Isaacson R, Kim HT, Silver PA, and Wagner G (2005). Ufd1 exhibits the AAA-ATPase fold with two distinct ubiquitin interaction sites. Structure 13, 995–1005. 10.1016/j.str.2005.04.013. [PubMed: 16004872]
16. Olszewski MM, Williams C, Dong KC, and Martin A (2019). The Cdc48 unfoldase prepares well-folded protein substrates for degradation by the 26S proteasome. Communications Biology 2, 29. 10.1038/s42003-019-0283-z. [PubMed: 30675527]
17. Ye Y, Blaser G, Horrocks MH, Ruedas-Rama MJ, Ibrahim S, Zhukov AA, Orte A, Klenerman D, Jackson SE, and Komander D (2012). Ubiquitin chain conformation regulates recognition and activity of interacting proteins. Nature 492, 266–270. 10.1038/nature11722 10.1038/nature11722. Epub 2012 Dec 2. [PubMed: 23201676]
18. Cook WJ, Jeffrey LC, Carson M, Chen Z, and Pickart CM (1992). Structure of a diubiquitin conjugate and a model for interaction with ubiquitin conjugating enzyme (E2). J Biol Chem 267, 16467–16471. [PubMed: 1322903]
19. Banerjee S, Bartesaghi A, Merk A, Rao P, Bulfer SL, Yan Y, Green N, Mroczkowski B, Neitz RJ, Wipf P, et al. (2016). 2.3 A resolution cryo-EM structure of human p97 and mechanism of allosteric inhibition. Science 351, 871–875. 10.1126/science.aad7974. [PubMed: 26822609]
20. Schuller JM, Beck F, Lossl P, Heck AJ, and Forster F (2016). Nucleotide-dependent conformational changes of the AAA+ ATPase p97 revisited. FEBS letters 590, 595–604. 10.1002/1873-3468.12091. [PubMed: 26849035]
21. Blythe EE, Gates SN, Deshaies RJ, and Martin A (2019). Multisystem Proteinopathy Mutations in VCP/p97 Increase NPLOC4.UFD1L Binding and Substrate Processing. Structure 27, 1820–1829 e1824. 10.1016/j.str.2019.09.011. [PubMed: 31623962]
22. Chin JW, Santoro SW, Martin AB, King DS, Wang L, and Schultz PG (2002). Addition of p-azido-L-phenylalanine to the genetic code of Escherichia coli. J Am Chem Soc 124, 9026–9027. [PubMed: 12148987]
23. Zhang M, Chang H, Zhang Y, Yu J, Wu L, Ji W, Chen J, Liu B, Lu J, Liu Y, et al. (2012). Rational design of true monomeric and bright photoactivatable fluorescent proteins. Nat Methods 9, 727–729. 10.1038/nmeth.2021. [PubMed: 22581370]
24. Sato Y, Tsuchiya H, Yamagata A, Okatsu K, Tanaka K, Saeki Y, and Fukai S (2019). Structural insights into ubiquitin recognition and Ufd1 interaction of Npl4. Nature communications 10, 5708. 10.1038/s41467-019-13697-y.
25. Tsuchiya H, Burana D, Ohtake F, Arai N, Kaiho A, Komada M, Tanaka K, and Saeki Y (2018). Ub-ProT reveals global length and composition of protein ubiquitylation in cells. Nature communications 9, 524. 10.1038/s41467-018-02869-x.
26. Carrion-Vazquez M, Li H, Lu H, Marszalek PE, Oberhauser AF, and Fernandez JM (2003). The mechanical stability of ubiquitin is linkage dependent. Nat Struct Biol 10, 738–743. 10.1038/nsb965. [PubMed: 12923571]
27. Dai RM, and Li CC (2001). Valosin-containing protein is a multi-ubiquitin chain-targeting factor required in ubiquitin-proteasome degradation. Nature cell biology 3, 740–744. 10.1038/35087056. [PubMed: 11483959]
28. Bard JAM, and Martin A (2018). Recombinant Expression, Unnatural Amino Acid Incorporation, and Site-Specific Labeling of 26S Proteasomal Subcomplexes. Methods Mol Biol 1844, 219–236. 10.1007/978-1-4939-8706-1_15. [PubMed: 30242713]

29. Worden EJ, Padovani C, and Martin A (2014). Structure of the Rpn11-Rpn8 dimer reveals mechanisms of substrate deubiquitination during proteasomal degradation. Nature Structural & Molecular Biology 21, 220–227. 10.1038/nsmb.2771 10.1038/nsmb.2771. Epub 2014 Jan 23.

30. Carvalho AF, Pinto MP, Grou CP, Vitorino R, Domingues P, Yamao F, Sa-Miranda C, and Azevedo JE (2012). High-yield expression in Escherichia coli and purification of mouse ubiquitin-activating enzyme E1. Molecular biotechnology 51, 254–261. 10.1007/s12033-011-9463-x 10.1007/s12033-011-9463-x. [PubMed: 22012022]

31. Mikolajczyk J, Drag M, Bekes M, Cao JT, Ronai Z, and Salvesen GS (2007). Small ubiquitin-related modifier (SUMO)-specific proteases: profiling the specificities and activities of human SENPs. J Biol Chem 282, 26217–26224. 10.1074/jbc.M702444200. [PubMed: 17591783]

32. Dong KC, Helgason E, Yu C, Phu L, Arnott DP, Bosanac I, Compaan DM, Huang OW, Fedorova AV, Kirkpatrick DS, et al. (2011). Preparation of distinct ubiquitin chain reagents of high purity and yield. Structure 19, 1053–1063. 10.1016/j.str.2011.06.010 10.1016/j.str.2011.06.010. [PubMed: 21827942]

Highlights:

- Cdc48-Ufd1/Npl4 engages substrates through rapid unfolding of an initiator ubiquitin
- Ufd1's UT3 domain is a linkage-specific sensor for an initiator-proximal ubiquitin
- Chains of 4-6 ubiquitins allow robust engagement through additional Npl4 interactions
- Processing of initiator-distal ubiquitins is rate-limiting for substrate release

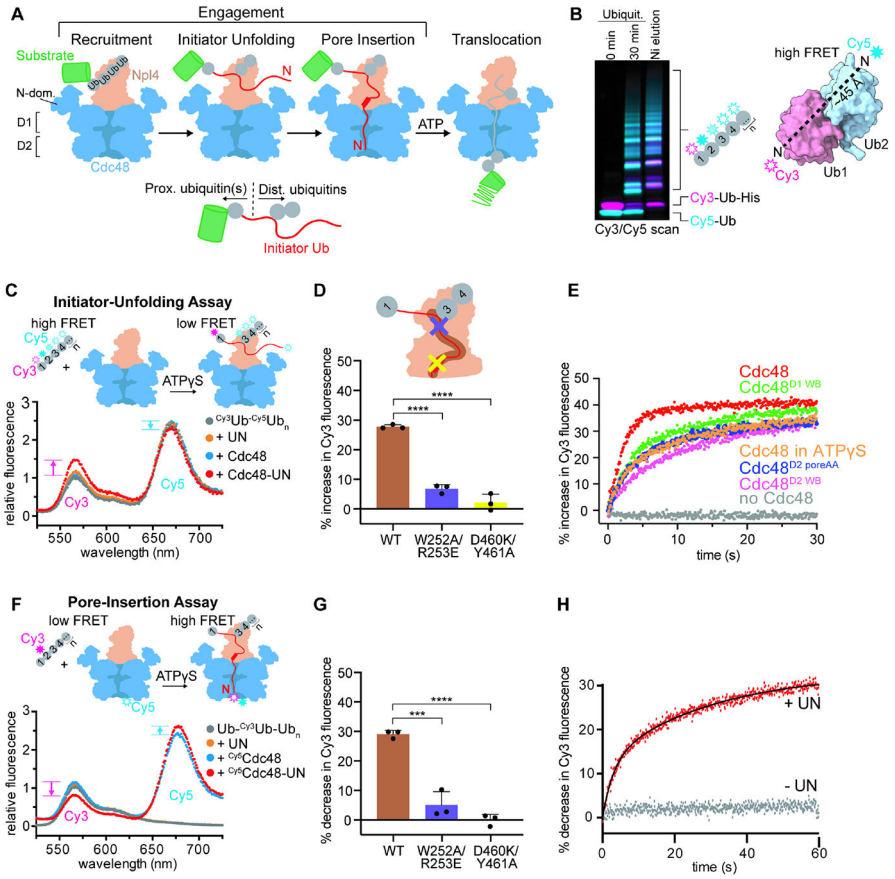

Figure 1. Cdc48-UN rapidly engages polyubiquitin chains in an ATP-hydrolysis-independent manner.

A) Top: Overview of the mechanism for engagement and processing of polyubiquitinated substrates by Cdc48-UN. A substrate (green) is targeted to Cdc48 (blue) through the recognition of attached polyubiquitin chains (gray) by the Npl4 (orange) and Ufd1 (not pictured) cofactor proteins. The ubiquitin serving as the initiator (red) unfolds and its N-terminus inserts into the Cdc48 pore. Following substrate engagement, Cdc48 uses ATP hydrolysis to translocate and unfold ubiquitins and the attached substrate polypeptide. Bottom: Schematic of a substrate during initiation, with the initiator ubiquitin shown in red. Relative to the initiator, ubiquitin moieties towards the substrate are proximal and ubiquitins on the other side are called distal. **B)** Left: SDS-PAGE analysis of the assembly and purification of polyubiquitin chains for FRET-based studies, which consist of a proximal Cy3-labeled ubiquitin and several Cy5-labeled distal ubiquitins. Double-labeled chains were visualized by Cy3 fluorescence (magenta) and Cy5 fluorescence (cyan). Right: The crystal structure of a K48-linked ubiquitin dimer (PDB ID: 1AAR) shows the distance between the Cy3-donor labeled N-terminus of the first ubiquitin in the chain and the Cy5-acceptor labeled N-terminus of the second ubiquitin in the chain. **C)** Fluorescence emission spectra after 480-nm excitation of ^{Cy3}Ub-^{Cy5}Ub$_n$ polyubiquitin chains incubated with Cdc48 and UN together or individually in ATPγS. Fluorescence intensity for each spectrum was normalized relative to the Cy3 emission maximum at 568 nm for the ^{Cy3}Ub-^{Cy5}Ub$_n$ alone, which was set to 1 (gray). Arrows indicate the direction of changes in Cy3- or

Cy5-fluorescence intensity when transitioning from a high-FRET to a low-FRET state upon initiator-ubiquitin unfolding. **D)** Mutations in Npl4's initiator-binding groove compromise the Cdc48-UN-mediated unfolding of an initiator ubiquitin within K48-linked chains. Bars represent the percent increase in steady-state Cy3-donor fluorescence when wild-type or mutant UN is present in a sample of ^{Cy3}Ub-^{Cy5}Ub$_n$ and Cdc48 in ATPγS. The mean and individual measurements are shown for N = 3 technical replicates. Statistical significance was calculated using a one-way ANOVA test: ****$p < 0.0001$. **E)** Kinetics of initiator unfolding within K48-linked polyubiquitin chains by Cdc48-UN under various conditions. Shown is the Cy3-donor fluorescence intensity following rapid stopped-flow mixing of ^{Cy3}Ub-^{Cy5}Ub$_n$ polyubiquitin chains with Cdc48-UN. Traces were normalized to the initial fluorescence signal determined by extrapolating the exponential fit to t = 0 s. Cdc48$^{D1\ WB}$ represents the ATP-hydrolysis deficient Walker B mutant with an E315Q substitution in the D1 domain, while Cdc48$^{D2\ WB}$ represents the ATP-hydrolysis deficient Walker B mutant with E588Q substitution in the D2 domain. Cdc48^{D2poreAA} represents a pore loop double mutant with W561A/Y562A substitutions in D2. **F)** Fluorescence emission spectra after 480-nm excitation of Ub-^{Cy3}Ub-Ub$_n$ polyubiquitin chains incubated with ^{Cy5}Cdc48 and UN together or individually in ATPγS. Fluorescence intensity for each spectrum was normalized relative to the Cy3 emission maximum at 568 nm for the Ub-^{Cy3}Ub-Ub$_n$ alone, which was set to 1 (gray). Arrows indicate the direction of changes in Cy3- or Cy5-fluorescence intensity during the transition from a low-FRET to high-FRET states upon pore insertion of the initiator ubiquitin. **G)** Cdc48-pore insertion of an initiator ubiquitin at the second position within a K48-linked polyubiquitin chains is reduced by mutations in Npl4's initiator-binding groove. Bars represent the percent increase in Cy3-donor fluorescence when wild-type or mutant UN is added to a sample of Ub-^{Cy3}Ub-Ub$_n$ and ^{Cy5}Cdc48 in ATPγS. The mean and individual measurements are shown for N = 3 technical replicates. Statistical significance was calculated using a one-way ANOVA test: ****$p < 0.0001$; ***$p = 0.001$. **H**) Pore-insertion kinetics for an initiator ubiquitin at the second position within K48-linked polyubiquitin chains entering Cdc48-UN in ATPγS. Shown is the decrease in Cy3-donor fluorescence intensity following rapid stopped-flow mixing of Ub-^{Cy3}Ub-Ub$_n$ polyubiquitin chains with ^{Cy5}Cdc48-UN. Traces were normalized to the initial fluorescence signal determined by extrapolation of the exponential fit to t = 0 s. See also Figure S1.

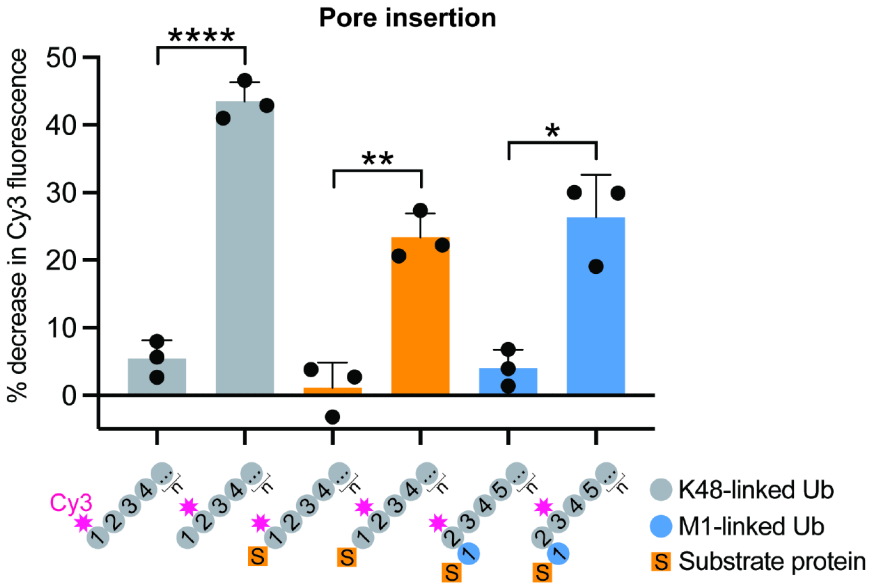

Figure 2. Initiator engagement requires a proximally located linkage-specific ubiquitin moiety.

Cdc48-pore insertion of an initiator ubiquitin located at the first or second K48-linked position within polyubiquitin-chain constructs. Bars represent the percent increase in Cy3-donor fluorescence when UN is present in a sample of Cy3-labeled chains and ^{Cy5}Cdc48 in ATPγS. Orange squares represent an SH3 domain fused to the C-terminus of the most proximal ubiquitin and blue circles indicate a ubiquitin fused linearly to the C-terminus of the most proximal K48-linked ubiquitin. The individual fluorescence values and their mean are shown for N = 3 technical replicates. Statistical significance was calculated using an unpaired two-tailed Welch's t-test: ****$p < 0.0001$; **$p = 0.0017$; *$p = 0.0144$. See also Figure S2.

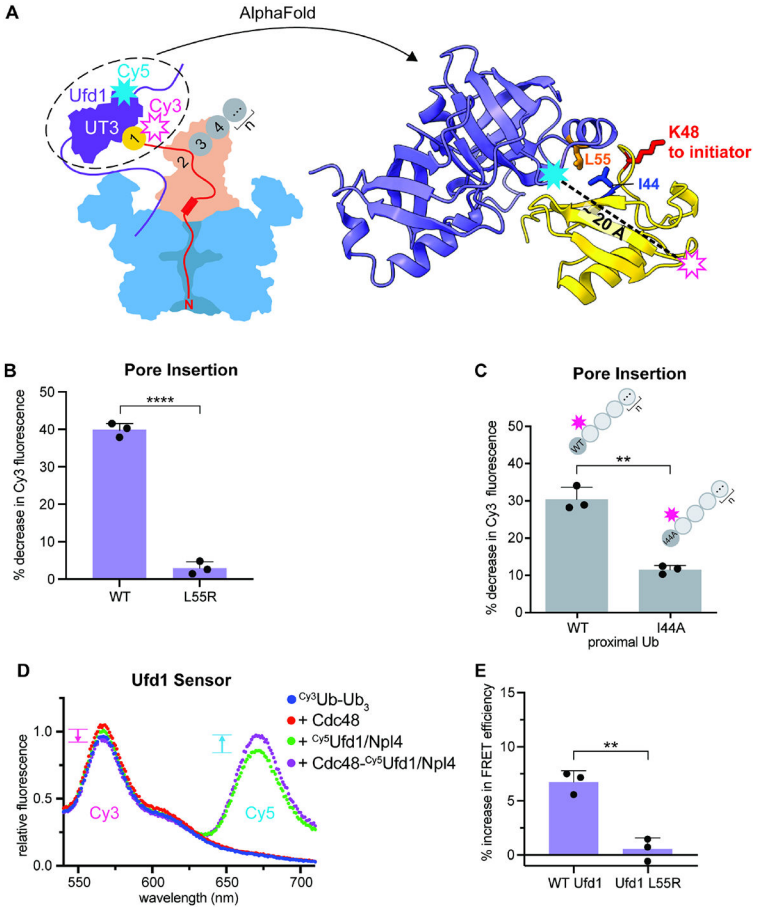

Figure 3. Ufd1's UT3 domain functions as a proximal ubiquitin sensor for efficient initiator unfolding and pore insertion.

A) Left: Schematic of Cdc48-UN with a ubiquitin moiety (yellow circle) proximal to the initiator ubiquitin (red line) interacting with the UT3 domain (purple) of the Ufd1 cofactor subunit. Placing a Cy3 donor dye on the N-terminus of this proximal ubiquitin and a Cy5 acceptor on UT3 (R64C) allows monitoring this interaction through FRET. Right: AlphaFold2/ColabFold model for the complex between a K48-linked ubiquitin and Ufd1's UT3 domain. I44 and K48 of ubiquitin, as well as the binding-relevant L55 of UT3 are depicted as blue, red, and orange sticks, respectively. For PAE plot see Fig. S3. **B)** The L55R mutation in Ufd1's UT3 domain strongly diminishes Cdc48-UN pore insertion of an initiator ubiquitin at the second position in a K48-linked polyubiquitin chain. Bars represent the percent decrease in Cy3-donor fluorescence when wild-type or L55R-mutant UN are present in a sample of Ub-^{Cy3}Ub-Ub$_n$ and ^{Cy5}Cdc48 in ATPγS. The individual fluorescence values and their mean are shown for N = 3 technical replicates. Statistical significance was calculated using an unpaired two-tailed Welch's t-test: ****$p < 0.0001$. **C**) Cdc48-UN insertion of a initiator ubiquitin at the second position in a ubiquitin chain carrying an I44A mutation in the most proximal moiety (Ub^{I44A}-^{Cy3}Ub-Ub$_n$) to disrupt ubiquitin binding to the UT3 domain of wild-type Ufd1. Statistical significance was calculated using an unpaired two-tailed Welch's t-test: **$p = 0.0052$. **D)** Fluorescence emission spectra after 480-nm excitation of ^{Cy3}Ub-Ub$_3$ polyubiquitin chains incubated with Cdc48 and ^{Cy5}UN

together or individually in ATPγS. Fluorescence intensity for each spectrum was normalized relative to the Cy3 emission maximum at 568 nm for ^{Cy3}Ub-Ub$_3$ alone, which was set to 1 (blue). Arrows indicate the direction of changes in Cy3- or Cy5-fluorescence intensity during the transition from a low-FRET to a high-FRET state upon binding of the most proximal ubiquitin to the UT3 domain of Ufd1. **E)** Binding of the most proximal ubiquitin in K48-linked Ub$_4$ chains to the UT3 domain of Cdc48-UN containing the Ufd1 L55R mutation. Bars represent the percent increase in apparent FRET efficiency when wild-type or L55R-mutant ^{Cy5}UN is mixed with ^{Cy3}Ub-Ub$_4$ and Cdc48 in ATPγS. Individual values and their mean are shown for N = 3 technical replicates. Statistical significance was calculated using an unpaired two-tailed Welch's t-test: **p = 0.0018. See also Figure S3 and S4.

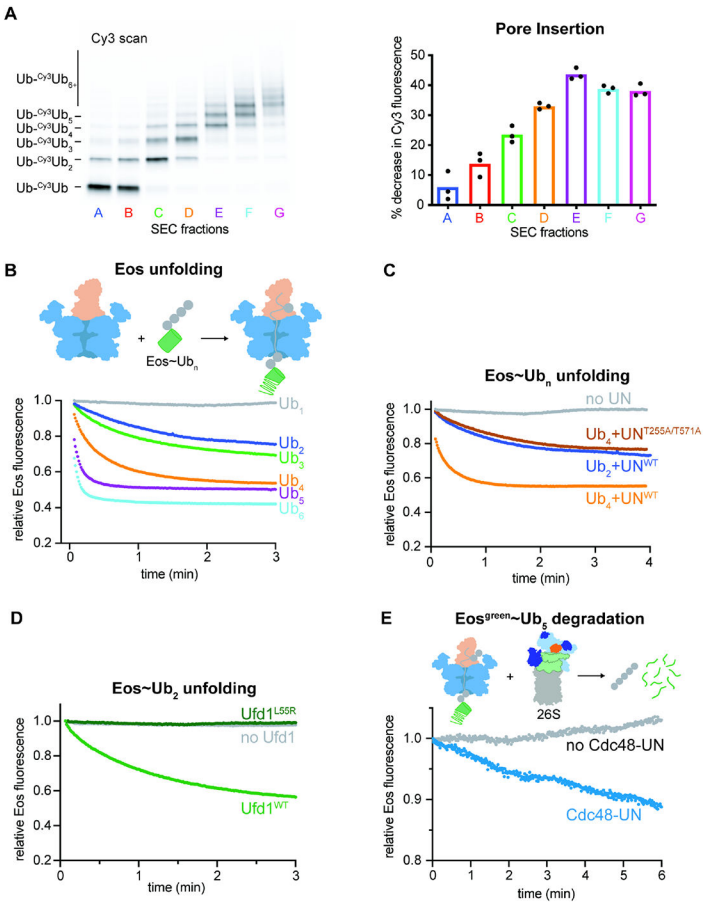

Figure 4. Npl4 binding of distal ubiquitins ensures robust initiator unfolding and engagement.

A) Left: SDS-PAGE analysis of size-exclusion chromatography (SEC) fractions for the separation of Ub-^{Cy3}Ub-Ub$_n$ ubiquitin chains, containing mixtures of various chain lengths and visualized by Cy3 fluorescence. Right: Dependence of the initiator insertion into the Cdc48-UN pore on the length of the K48-linked polyubiquitin chain. Bars represent the percent decrease in Cy3-donor fluorescence when UN is present in a sample consisting of one Ub-^{Cy3}Ub-Ub$_n$ SEC fraction A-G (shown in the gel at the right) and ^{Cy5}Cdc48 in ATPγS. Individual fluorescence values and their mean are shown for N = 3 technical replicates. **B)** Cdc48-UN mediated unfolding of mEos3.2 substrates with attached K48-linked chains of lengths Ub$_1$ to Ub$_6$. Shown is the decay of Eos-fluorescence intensity after mixing Eos~Ub$_n$ with Cdc48-UN. Unfolding traces were normalized to the initial fluorescence signal determined by extrapolating the exponential fits to t = 0 s. **C)** Traces for the unfolding of Eos~Ub$_2$ and Eos~Ub$_4$ in the presence of Cdc48-UN with wild-type Npl4 are compared to the unfolding of Eos~Ub$_4$ by Cdc48-UN containing a double-mutant Npl4 (T255A/T571A) with defective tower ubiquitin-binding sites (brown curve). **D)** Unfolding of an Eos substrate with an attached K48-linked Ub$_2$ chain by Cdc48-UN containing Ufd1 L55R. Shown is the decay of Eos-fluorescence intensity after mixing of Eos~Ub$_2$ with Cdc48-UN. Traces were normalized to the initial fluorescence signal determine by extrapolating the exponential fit to t = 0 s. **E)** Proteasomal degradation of Eos^{green}~Ub$_5$ after prior unfolding by Cdc48-UN. Shown are the changes in fluorescence when Eos^{green}~Ub$_5$

is mixed with the 26S proteasome after pre-incubation in the absence or presence of Cdc48-UN. See also Figure S5-S7.

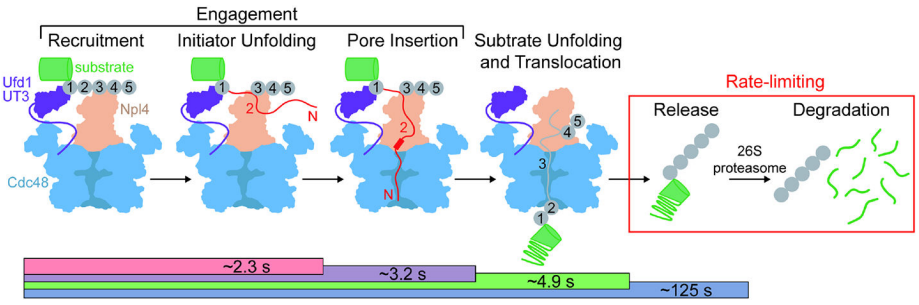

Figure 5. Model of substrate engagement and processing by Cdc48-UN.

Ubiquitin engagement and translocation, as well as unfolding of the attached substrate protein are rapid relative to the release of the ubiquitinated substrate from Cdc48-UN, which is thus rate-limiting for Cdc48-mediated degradation by the 26S proteasome in the absence of any other cofactors. The bars at the bottom report observed total time constants including all previous steps for substrate processing in the presence of ATP, except for pore insertion, which was measured in the presence of ATPγS. See also Figure S7.

Table 1.

Kinetics of initiator-ubiquitin unfolding.

Time constants for the fast and slow phases during single-turnover unfolding of the initiator ubiquitin moiety in ^{Cy3}Ub-^{Cy5}Ub$_n$ by Cdc48-UN and its Walker-B or pore-loop mutants in the presence of ATP or ATPγS, as determined by double-exponential fitting of the Cy3-fluorescence increase shown in Fig. 1E. Listed are also the amplitudes of the fast phase (mean values and S.D. for N = 3 technical replicates).

Cdc48 variant	**τ_{fast} (s) Mean ± S.D.**	**τ_{slow} (s) Mean ± S.D.**	**Fast-phase amplitude (%) Mean ± S.D.**
WT, ATP	2.3 ± 0.2	-	100
WT, ATPγS	2.7 ± 0.2	21.5 ± 1.0	48.9 ± 2.2
D1 Walker B (E315Q), ATP	3.0 ± 0.1	25.2 ± 2.2	55.6 ± 2.3
D2 Walker B (E588Q), ATP	3.8 ± 0.5	25.6 ± 1.1	38.6 ± 0.8
D2 pore loop (W561A/Y562A), ATP	2.6 ± 0.5	18.5 ± 2.8	53.6 ± 1.3

Table 2.

Kinetics of mEos3.2 unfolding depending on the ubiquitin-chain length.

Time constants for the fast phase of green Eos unfolding by Cdc48-UN under single-turnover conditions and time constants for the multiple-turnover unfolding of photoconverted red Eos as a function of the attached ubiquitin-chain length (mean values and S.D. for N = 3 technical replicates). Values for the multiple-turnover unfolding of Eos~Ub_2 and Eos~Ub_4 were determined by Michaelis-Menten analyses, see Fig. S6B.

Ub_n-Eos	**τ_{fast} (s) Single turnover Mean ± S.D.**	**τ_{fast} (s) Multiple turnover Mean ± S.D.**
Eos~Ub	-	-
Eos~Ub_2	79.3 ± 2.3	95 ± 5
Eos~Ub_3	61.8 ± 5.0	N.D.
Eos~Ub_4	12.8 ± 0.9	94 ± 4
Eos~Ub_5	4.9 ± 1.2	125 ± 4
Eos~Ub_6	4.4 ± 0.1	N.D.

KEY RESOURCES TABLE

REAGENT or RESOURCE	SOURCE	IDENTIFIER
Bacterial and virus strains		
Escherichia coli: BL21 Star (DE3) strain	QB3 MacroLab (UC Berkeley)	N/A
Chemicals, peptides, and recombinant proteins		
Sulfo-Cyanine3 maleimide	Lumiprobe	CAT# 21380
Sulfo-Cyanine5 maleimide	Lumiprobe	CAT# 23380
Sulfo-Cyanine5 DBCO	Lumiprobe	CAT# 233F0
4-Azido-L-phenylalanine HCl	Acrotein ChemBio Inc.	CAT#A-7137
Deposited data		
Mendeley Data dataset: Uncropped SDS-PAGE gel images scanned for Cy3/C5 fluorescence or Coomassie stain	This paper	doi:10.17632/65dyy7tkny.1
Recombinant DNA		
Plasmid: His_6-3C-Cdc48 (AMP)	Olszewski et al Comm Bio 2019	pAM282
Plasmid: His_6-3C-Cdc48^{E315Q} (AMP)	This paper	pAM283
Plasmid: His_6-3C-Cdc48^{E588Q} (AMP)	This paper	pAM284
Plasmid: His_6-3C-Cdc48$^{W561A/Y562A}$ (AMP)	This paper	pAM285
Plasmid: His_6-3C-Cdc48^{D602AzF}-Avi (AMP)	This paper	pAM286
Plasmid: AzF tRNA synthetase (SPEC)	This paper	pAM293
Plasmid: Ufd1-3C-His_6 (KAN)	Olszewski et al Comm Bio 2019	pAM294
Plasmid: Ufd1^{R64C}-3C-His_6 (KAN)	This paper	pAM295
Plasmid: Ufd1^{L55R}-3C-His_6 (KAN)	This paper	pAM296
Plasmid: Npl4 (AMP)	Olszewski et al Comm Bio 2019	pAM287
Plasmid: Npl4$^{W252A/R253E}$ (AMP)	This paper	pAM288
Plasmid: Npl4$^{D460K/Y461A}$ (AMP)	This paper	pAM289
Plasmid: His_6-GST-3C-Npl4 (AMP)	This paper	pAM290
Plasmid: His_6-GST-3C-Npl4$^{T255A/T571A}$ (AMP)	This paper	pAM291
Plasmid: Ub (KAN)	This paper	pAM297
Plasmid: MC-Ub (KAN)	This paper	pAM298
Plasmid: MC-Ub-3C-His_6 (KAN)	This paper	pAM299
Plasmid: MC-Ub^{I44A}-3C-His_6 (KAN)	This paper	pAM300
Plasmid: MC-Ub-SH3-3C-His_6 (KAN)	This paper	pAM301
Plasmid: MC-Ub-Ub^{K48R}-SH3-3C-His_6 (KAN)	This paper	pAM302
Plasmid: His_6-GG-Ub^{K48R} (KAN)	This paper	pAM303
Plasmid: His_6-SUMO-Ub-mEos3.2-intein-CBD (AMP)	This paper	pAM292
Plasmid: His_6-TEV-gp78RING-Ube2g2 (KAN)	Blythe PNAS 2017	pAM304
Plasmid: His_6-mEos3.2-Ub^{K48R} (KAN)	This paper	pAM305

REAGENT or RESOURCE	SOURCE	IDENTIFIER
Plasmid: His_6-SUMO-Ub-mEos3.2-mTurquoise2-intein-CBD (AMP)	This paper	pAM358
Plasmid: Ube1 (KAN)	Gift from Jorge Eduardo Azevedo	Addgene plasmid # 32534)
His_6-SENP2 (KAN)	Gift from Guy Salvesen	Addgene plasmid # 16357
Plasmid: His-Cdc34 (KAN)	This paper	pAM359
Plasmid: His-GST-PreScission (AMP)	Gift QB3 MacroLab	pAM050
Plasmid: USP2	Gift from Cheryl Arrowsmith	Addgene plasmid # 36894
Software and algorithms		
Prism 9.3.1	GraphPad Software	N/A
PyMOL Molecular Graphics System 2.5.2	Schrödinger, LLC	N/A
Image Lab 6.1.0	Bio-Rad	N/A
AlphaFold2 in Google CoLab	DeepMind and Google	N/A